SPATIAL DISTRIBUTION OF IONIZED GAS IN BRIGHT BARRED SPIRAL GALAXIES: Hα IMAGES[1]

J.A. García-Barreto[2], J. Franco[2], R. Carrillo[2],
S. Venegas[3], and B. Escalante-Ramírez[3]

RESUMEN

El presente trabajo estudia la distribución global del gas ionizado en galaxias espirales con barra. El enfoque principal es detectar estructuras simétricas como lo serían las llamadas estructuras circunnucleares. Para este propósito se presentan las imágenes de 52 galaxias espirales con barra y brillantes, usando el filtro angosto que incluye la emisión de Hα y también usando el filtro ancho en la banda *I*. Las galaxias se han seleccionado del Catálogo Shapley Ames con características de formación estelar reciente, dadas por su emisión de infrarrojo lejano del satélite *IRAS*, es decir, con una temperatura de polvo mayor o igual que 25 K. Treinta y dos galaxias presentan emisión de Hα de sus regiones centrales, pero la emisión proveniente de estructuras circunnucleares solo se observó en diez galaxias. Aproximadamente la mitad de las galaxias observadas muestran emisión de Hα de varias regiones en el disco y dieciocho muestran emisión de Hα en la región de la barra (estelar). La emisión de gas ionizado es fácilmente detectada en algunas galaxias de anillos internos y externos. Otras galaxias muestran estructuras de gas ionizado más complejas probablemente debido a fuerzas de marea de galaxias cercanas.

ABSTRACT

CCD images of a set of 52 bright barred spiral galaxies in the narrow band filter Hα and in the broadband *I* filter are presented. The sample was selected from the Shapley Ames Catalog, with *IRAS* fluxes characteristic of star formation and a dust temperature above $T_d \geq 25$ K. The study is aimed at identifying the global distribution and the underlying symmetries of the structures of ionized gas in barred galaxies. Thirty-two galaxies present Hα emission from the innermost central regions, but the emission from nuclear rings is observed only in ten galaxies. About half of the observed galaxies show Hα emission from several regions in the disk, and 18 galaxies display emission from along the bar. The Hα emission from inner and outer rings are easily identified in some galaxies. Some other galaxies present a more complicated spatial distributions, probably due to tidal or direct encounters with neighboring galaxies.

Key words: **GALAXIES – ISM — GALAXIES – SPIRAL — GALAXIES – STRUCTURE**

1. INTRODUCTION

Studies of the spatial distribution of the light in barred spiral galaxies show a series of symmetric structures at different radii known as nuclear rings, inner rings, outer rings, and pseduo-rings (Buta 1986, 1995; Buta & Crocker 1991). The name *ring* is associated with the optical appearance of the structure on the plane of the sky rather than to an intrinsic morphological structure. The origin of these features is probably controlled by the non-axisymmetric gravitational potential of the bar (e.g., Lindblad 1958; Lynden-Bell & Kalnajs 1972; Contopoulos 1980; Athanassoula 1984; Contopoulos & Grösbol 1989). The dynamics under a non-axisymmetric po-

[2] Instituto de Astronomía, Universidad Nacional Autónoma de México.
[3] División de Estudios de Posgrado, Fac. de Ingeniería, Universidad Nacional Autónoma de México.

tential results in density enhancements at resonant radii called Lindblad Resonances (Lindblad 1958). In particular structures forming around the compact nucleus, generally known as nuclear rings, most probably are at a radius where an Inner Lindblad Resonance (ILR) would be predicted.

Nuclear rings are located at the innermost central regions of the host galaxies, but are difficult to detect in broadband optical images because of the small light contrast between the ring and the nearby galactic components (i.e., the nucleus, the bulge, and the stellar bar). The intense UV photon field produced by these massive stars ionize the surrounding medium, and a strong Hα emission is expected at the location of the ring. Hence, one can use Hα as a tracer of ring structures with star formation, and several nuclear rings have been found with emission-line, continuum-free, Hα images; i.e., NGC 1097 (Hummel, van der Hulst, & Keel 1987), NGC 3351 (Kenney et al. 1992), and NGC 4321 (Arsenault et al. 1988).

The present study is aimed at deriving the general features of the ionized gas, in particular in finding new nuclear rings, in *barred galaxies*. Our data show the spatial distribution of Hα emission in a field of view of $\sim 4'$ which, we believe, is an important tool to understand the dynamics of the gaseous disk in the presence of a non-axisymmetric gravitational potential. We have detected 10 out of 52 galaxies with extended Hα emission that could be associated with nuclear rings. Our study is focused on bright barred spiral galaxies and is complementary to other studies of the morphology of ionized gas in normal galaxies, as those reported by Hodge & Kennicutt (1983), Keel (1983), Pogge (1989), Ryder & Dopita (1993), and Nordgren et al. (1995). Our set of galaxies was chosen to include bright and nearby barred galaxies

visible from the northern sky and is by no means a complete set neither in magnitude nor in volume. In § 2 we describe the equipment, convolution algorithm, procedures, and results. In § 3 we discuss the spatial distribution of the ionized gas, and our conclusions are summarized in § 4.

2. OBSERVATIONS AND RESULTS

The optical observations were carried out at the Observatorio Astronómico Nacional in San Pedro Mártir, Baja California, México. We used the 2.12-m telescope f/7.5, in June 1992 and December 1993, equipped with a CCD detector of 1024×1024 pixels and the broadband Johnson filter I and the narrowband Hα, under good seeing conditions ($\simeq 1$ to 1.3''). Our Hα images also include the [N II] emission lines since our narrow filter had a FWHM of 89 Å. A log of the observations and a list of the characteristics of the filters are presented in Table 1.

The images were bias subtracted and then flat-

TABLE 1

FILTERS USED IN THE CCD IMAGES[a]

Filter	Central λ Å	$\Delta\lambda$ Å	Exposure Time (sec)
I	8040	1660	60
Hα_0	6459	101	300
Hα_1	6607	89	300

[a] Observations on June 1, 1992 and December 15, 1993.

TABLE 2

PROPERTIES OF OBSERVED GALAXIES

Galaxy NGC /IC	Type	R.A. (1950.0) Dec. h m s	o ' ''	IRAS Fluxes (Jy) 12μ	25μ	60μ	100μ	P.A. Bar[a] E of N
N 672	SBc(s)	01 45 05	+27 11 06	0.25	0.37	3.37	8.34	105
N 1022	SBa(r)pe[c]	02 36 04	−06 53 24	0.75	3.26	20.12	27.44	115
N 1326	RSBa	03 22 01	−36 38 24	0.27	0.79	8.31	14.30	20
I 1953	SBbc(rs)	03 31 29	−21 38 36	0.25	0.93	8.68	11.48	150
N 1415	SBa	03 38 47	−22 43 24	0.26	0.55	5.28	12.32	130
N 1637	SBc(s)	04 38 58	−02 57 06	0.33	0.98	5.73	13.78	75
N 1784	SBbc(r)	05 03 07	−11 56 24	0.25	0.35	2.44	9.30	90
N 1832	SBb(r)	05 09 48	−15 44 48	0.31	0.58	6.70	17.11	165

TABLE 2 (CONTINUED)

Galaxy NGC /IC	Type	R.A. (1950.0) Dec.					IRAS Fluxes (Jy)				P.A. Bar[a]
		h	m	s	o	'	"	12μ	25μ	60μ	100μ	E of N

Galaxy NGC /IC	Type	h m s	o ' "	12μ	25μ	60μ	100μ	E of N
N 2139	SBc(s)	05 59 04	−23 40 18	0.30	0.63	6.64	14.03	90
N 2217	SBa(s)	06 19 41	−27 12 30	0.25	0.25	0.98	5.07	110
N 2223	SBbc(r)	06 22 31	−22 48 42	0.25	0.25	0.65	3.59	40
N 2339	SBc(s)	07 05 25	+18 51 42	0.53	2.11	18.96	32.24	70
N 2525	SBc(s)	08 03 15	−11 17 06	0.25	0.57	6.08	16.76	70
N 2545	SBbc(r)	08 11 20	+21 30 24	0.25	0.33	0.89	2.80	170
N 2798	SBa(s)	09 14 10	+42 12 42	0.76	3.11	22.76	29.13	40
N 2787	SBa(s)	09 14 50	+69 24 54	0.63	0.64	0.66	2.05	160
N 2835	SBc(rs)	09 15 37	−22 08 48	0.25	0.25	2.56	14.40	110
N 3185[c]	SBa(s)	10 14 54	+21 56 18	0.25	0.29	1.58	3.68	110
N 3287	SBc(s)	10 32 04	+21 54 30	0.25	0.83	1.59	5.03	20
N 3318	SBbc(rs)	10 35 03	−41 22 06	0.35	0.56	4.97	12.65	170
N 3319	SBc(s)	10 36 14	+41 56 48	0.25	0.34	0.69	2.67	40
N 3351	SBb(r)	10 41 19	+11 58 06	0.57	1.91	17.37	35.30	110
N 3359	SBc(s)pec	10 43 21	+63 29 12	0.25	0.21	4.06	14.32	5
N 3367[d]	SBc(s)	10 43 56	+14 00 48	0.44	1.07	5.90	13.01	70
N 3504	SBb(s)	11 00 29	+28 14 30	1.04	3.72	19.17	32.89	145
N 3513	SBc(s)	11 01 20	−22 58 36	0.25	0.25	2.63	7.63	120
N 3783[b]	SBa(r)	11 36 33	−37 27 42	0.77	2.43	3.37	5.12	160
N 3912	SB(late)p	11 47 30	+26 45 18	0.25	0.40	3.40	6.56	15
N 4123	SBbc(rs)	12 05 38	+03 09 18	0.40	1.21	5.98	10.96	105
N 4314	SBa(rs)p	12 20 02	+30 10 20	0.25	0.39	3.76	7.59	145
N 4385	SBbc(s)	12 23 12	+00 50 54	0.35	1.08	4.66	6.13	100
N 4435	SB0	12 25 08	+13 21 24	0.25	0.75	2.07	4.15	15
N 4477	SBa	12 27 31	+13 54 42	0.35	0.55	0.59	1.11	15
N 4507[c]	SBab(rs)	12 32 55	−39 38 00	0.46	1.41	4.58	5.60	50
N 4561	SBc	12 33 38	+19 36 06	0.25	0.37	1.22	2.68	120
N 4688	SBc(s)	12 45 14	+04 36 36	0.25	0.38	0.99	2.16	35
N 4691	RSB/S0p	12 45 39	−03 03 39	0.71	2.43	15.18	21.64	85
N 5135[c]	SBb	13 22 56	−29 34 18	0.67	2.48	16.18	30.83	125
N 5188	SBbc(s)	13 28 37	−34 32 00	0.75	2.79	22.73	35.44	50
N 5347[c]	SBb(s)	13 51 04	+33 44 12	0.29	0.92	1.44	2.71	100
N 5430	SBb(r)	13 59 09	+59 34 06	0.52	1.64	10.40	20.49	145
N 5534	SBbc(s)	14 15 01	−07 11 12	0.28	0.79	4.83	7.12	80
N 5597	SBc(s)	14 21 42	−16 32 12	0.46	1.40	8.70	15.32	55
N 5691	SBb pec	14 35 20	−00 10 54	0.25	0.45	3.43	6.60	90
N 5728[c]	SBb(s)	14 39 37	−17 02 18	0.32	0.81	8.40	15.17	35
N 5757	SBb(rs)	14 44 57	−18 52 06	0.48	0.91	6.19	13.10	165
N 5915	SBbc(s)p	15 18 48	−12 54 54	0.43	1.35	10.81	16.02	90
N 6239	SBc pec	16 48 31	+42 49 24	0.25	0.38	3.47	6.21	115
N 6907	SBbc(s)	20 22 07	−24 58 18	0.63	1.27	13.36	30.33	45
N 6951	SBb(rs)	20 36 37	+65 55 54	0.45	1.17	13.49	37.14	85
I 5273	SBc(s)	22 56 40	−37 58 24	0.25	0.46	4.44	11.47	45
N 7479[c]	SBbc(s)	23 02 26	+12 03 09	0.75	3.32	12.12	24.93	10

[a] Position angle of the bar is measured east of north with an estimated error of ±5°.
[b] Galaxy classified as Seyfert 1.
[c] Galaxies classified as Seyfert 2.
[d] Galaxy classified as Seyfert—like.

fielded with the NOAO IRAF software, by using an average of three 5-second exposures of blank fields taken at twilight or sunrise. Different flats were obtained for each filter. Images with the $H\alpha_0$ and $H\alpha_1$ filters were used as the continuum and continuum plus line emission, respectively, each with 300 seconds of exposure time. Images with I filters were obtained with an exposure time of 60 seconds each. All images were calibrated and edited for cosmic rays. The final $H\alpha$ images were obtained by subtracting the continuum, and are presented with north at the top and east to the left. For the subtraction, we first aligned the line+continuum and continuum images with field stars and used a 1:1 scale. After the subtraction, the field stars disappeared completely from the $H\alpha$ images. No amplitude calibration was performed in any of the filters, so no fluxes or magnitudes could be derived.

2.1. Selected Galaxies

From the early far-infrared $IRAS$ and radio continuum detections of spirals, Hawardeen et al. (1986) noticed that the central regions of barred galaxies had higher fluxes than the ones of normal spirals. Further studies in some particular barred galaxies indicated that there were bursts of star formation in their central regions, and these bursts seem to actually define the nuclear rings.

The galaxies studied here were selected in order to derive additional evidence for ionized gas structures in barred galaxies, and the sample was chosen with the following criteria: 1) bright barred galaxies in the Shapley Ames Catalog (first or second edition; Sandage & Tamman 1981), 2) with $IRAS$ colors characteristic of star-forming galaxies according to Helou (1986); that is, with $\log(f[12]/f[25]) \leq -0.15$ and $\log(f[60]/f[100]) \leq -0.1$, or equivalently an $IRAS$ dust temperature $\overline{T_d} \geq 25$ K, 3) be observable from our observatory, $-41° \leq \delta \leq +70°$. Table 2 list the observed galaxies. Table 3 list additional properties of the sample, including distances, inclinations, group association, dust temperatures, blue magnitudes, H I masses, ratios of X-ray to B luminosities, radio continuum fluxes at 20 and 6 cm, and $H\alpha$ fluxes through different apertures reported in the literature.

2.2. Convolution Algorithm

The final images in the narrowband $H\alpha$ filter and broadband I filter were processed with an algorithm designed to enhance the emitting regions in the CCD images. The algorithm was developed initially for noise reduction in tomography images and is based on a technique called polynomial transform (Escalante-Ramírez & Martens 1992). The algorithm does not explicitly use the point spread function of the system. It is an algorithm that first carries out

TABLE 3

ADDITIONAL PROPERTIES OF OBSERVED GALAXIES

Galaxy	D	i	T_d^a			L_X/L_B	S_{20}^b	S_6^c	$F(H\alpha)^d$	
NGC/IC	Mpc	°	Tully Group	K	log B	log M_H	10^{-5}	mJy	mJy	10^{-15}	Apert.^{e}
N 672	7.5	70	17−5+5	32	10.16	9.93	2.6	13.9	...	2754	7′
N 1022	18.5	28	52−1+1	40	9.87	8.34	...	40.9	21	724	3′
N 1326	16.9	53	51−1+1	37	10.13	9.26	...	30.6	14	1380	20″
I 1953	22.1	33	51−0+4	41	10.00	9.22	...	1.7	...	...	...
N 1415	17.7	65	51−4+4	33	9.73	...	...	26.0	...	...	...
N 1637	8.9	39	53−20+20	33	9.52	9.11	...	16.5	...	2089	3′
N 1784	28.7	55	34+5+4	28	10.34	10.11	31.2	...	...	...	...
N 1832	23.5	60	34−3+3	32	10.26	9.50	...	...	...	2399	3′
N 2139	22.4	53	34+1	34	10.16	9.80	...	...	...	2884	2′
N 2217	19.5	26	34−1+1	26	10.26	9.38	...	29.7	...	...	...
N 2223	33.7	...	34−8+8	25	10.53	9.91	...	...	...	...	...
N 2339	30.9	45	30+1	37	10.50	9.86	...	...	36	...	...
N 2525	21.1	45	31−0	31	10.15	9.20	28.5	...	...	...	...
N 2545	...	...	...	30	...	...	...	...	...	...	...
N 2798	27.1	75	21−6+16	42	10.06	...	...	71.6	37	...	...
N 2787	13.0	52	12−0	30	9.76	...	...	...	...	18	≤8″
N 2835	10.8	48	54−3+1	25	10.06	9.64	6.5	18.2	12	...	...
N 3185	21.3	55	21−6+6	33	9.76	...	...	...	...	199	3′
N 3287	20.6	64	21−6	30	9.78	...	...	...	...	...	...
N 3318	37.9	61	31−6+6	32	10.59	...	...	...	...	...	...

TABLE 3 (CONTINUED)

Galaxy NGC/IC	D Mpc	i °	Tully Group	T_d^a K	log B	log M_H	L_X/L_B 10^{-5}	S_{20}^b mJy	S_6^c mJy	$F(H\alpha)^d$ 10^{-15}	Apert.[e]
N 3319	11.5	57	15+7+7	28	9.68	9.41	...	11.5	...	...	...
N 3351	8.1	56	15−1	35	9.90	8.92	9.4	47.8	30	4570	7′
N 3359	19.2	55	12−0+1	29	10.43	10.27	...	50.1	15	...	...
N 3367	43.6	19	32−4+4	34	10.68	9.78	58.4	98.5		3361	≤94″
N 3504	26.5	35	21−7+7	37	10.34	8.77	40.9	265.0	117	3467	3′
N 3513	17.0	38	54−5+5	31	9.98	9.23	...	16.1	9	...	...
N 3783	38.5	23	31+11+10	39	10.40	9.55	7766.0	...	...	134	≤20″
N 3912	30.0	58	13−9+9	35	10.03	9.16	...	...	...	...	...
N 4123	25.3	39	22−11+11	36	10.29	9.95	...	22.0	12	347	≤8″
N 4314	9.7	15	14−1+1	35	9.65	6.6	...	11.0	5	55	≤8″
N 4385	33.5	56	11−25+24	41	10.10	9.23	209.4	...	...	...	...
N 4435	16.8	44	11−1	35	10.00	8.2	53.6	...	...	...	...
N 4477	16.8	26	11−1	36	10.14	8.1	45.7	...	...	...	...
N 4507	45.0	...	...	42	10.36	...	107.0	...	...	...	...
N 4561	12.3	25	11−0+1	34	9.30	8.96	...	...	...	513	2′
N 4688	17.1	...	11+2+1	34	9.50	9.4	...	...	...	...	...
N 4691	22.5	32	11−0+10	40	10.24	8.7	...	47.5	28	...	...
N 5135	53.2	...	...	35	10.64	10.2	64.7	...	...	...	...
N 5188	32.9	74	11−32+32	38	10.39	9.17	...	...	...	...	...
N 5347	36.7	37	42−0+1	36	9.98	9.58	...	...	...	...	...
N 5430	(38)	...	...	35	...	...	...	51.3	29	...	...
N 5534	(35)	...	...	39	...	...	...	...	...	...	...
N 5597	38.6	0	41−14+14	36	10.46	...	...	45.5	...	...	...
N 5691	30.2	34	41−2+1	35	10.19	...	...	...	...	...	...
N 5728	42.2	65	41+15+15	36	10.86	9.61	42.4	60	...	...	...
N 5757	39.5	32	41+15+15	34	10.46	...	...	38.9	...	...	...
N 5915	33.7	42	41−10+10	39	10.53	9.69	...	48.2	...	...	...
N 6239	18.9	67	44−0	36	9.76	8.69	...	...	...	...	...
N 6907	(42)	...	...	33	...	10.36	...	136	59	...	...
N 6951	24.1	28	40−0	31	10.48	9.68	35.3	...	32	...	...
I 5273	16.0	53	61−0+16	32	9.92	9.02	...	33.4	...	...	...
N 7479	...	...	...	34	...	...	...	109	46	1380	3′

[a] Dust temperature computed from *IRAS* FIR fluxes assuming $S_\nu \simeq \lambda^{-1}$ (García-Barreto et al. 1993).

[b] Radio continuum flux at 20 cm from Condon 1987; Condon et al. 1990.

[c] Radio continuum flux at 6 cm from Condon et al. 1991; García-Barreto et al. 1991a,b,c, 1993.

[d] Hα fluxes. Large aperture (2 to 7 ′) from Kennicutt & Kent 1983; from the nuclei of galaxies ($\leq 8''$) from Keel et al. 1985. Hα fluxes from NGC 1326 and NGC 3367 are taken from García-Barreto et al. 1991a, 1996. Units are $F(H\alpha)$ in 10^{-15} ergs cm^{-2} s^{-1}.

[e] Optical aperture of the Hα measurements or diameter from which flux has been measured.

an analysis of the extent and brightness of the structures, according to the intensity of each pixel with a variable window width and following the intensity changes among adjacent pixels. The resulting structures and noise levels are determined at each step. At the end, it does a synthesis process adaptively reconstructing the image according to the relevant image structures found in each window width. An example of how the convolution algorithm works and reproduces well galaxy structures is shown in Figure 1. The image in Fig. 1a is the direct CCD Hα continuum-free image of the galaxy NGC 3783. In this image one can hardly see the emission from the nucleus or from a ring-like structure. The image in Fig. 1b is the CCD image after being deconvolved with the polynomial algorithm. The central emission is recovered, and most notably a ring is now clearly seen in this deconvolved image. Also, one
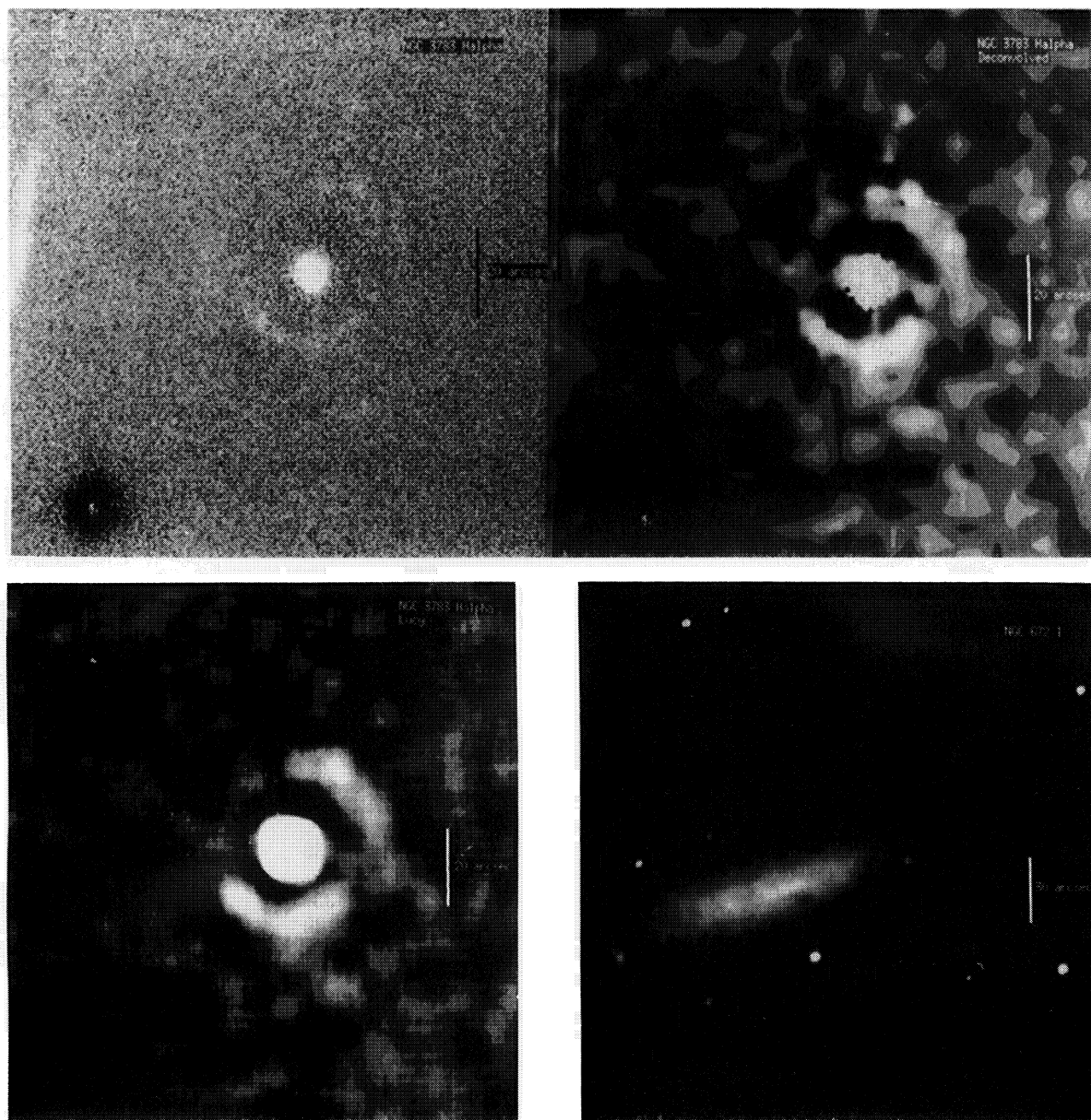
Fig. 1. *a*) CCD direct image of the Hα emission from the galaxy NGC 3783. The image has been flat-fielded, bias-corrected, and edited for cosmic rays. Continuum emission has been subtracted. The black image at the bottom left corner indicates that the subtraction was done correctly to eliminate the emission from forefront bright stars. The vertical line at the right side of the image shows the spatial scale of 20″. Hα emission from the galaxy is observed from the compact nucleus and weakly from a ring-like structure. *b*) Resulting image after deconvolving the direct CCD image in 1*a* with the polynomial transform algorithm. Notice that the emission from the compact nucleus and the ring-like structure is recovered but there is more structure visible now, specifically emission from regions connecting the compact nucleus with the ring-like structure at PA∼90°, ∼180°, and ∼260°. All of these structures were detected previously by Forte et al. (1987) and by Winge et al. (1992). There is also extended emission to the SW. *c*) Resulting image after deconvolving the direct CCD image 1*a* with the Lucy-Richardson algorithm. Notice that the basic emissions from the compact nucleus, the ring-like structure and the emissions at PA∼90°, ∼180°, and at ∼260° are all reproduced as in 1*b*. The extended emission to the SW is also seen with this algorithm which suggests that the emission is probably true. *d*) *I* broad band image of the barred galaxy NGC 672. In all images north is up, east is left.

sees emission apparently connecting the nucleus with the ring at a PA almost perpendicular to the bar, at PA $\sim 90°$, at PA $\sim 180°$, and at PA $\sim 260°$. The emission perpendicular to the bar has been already reported by Forte et al. (1987) and Winge et al. (1992), who referred to it as "the bridge". As a comparison, the image in Fig. 1c is the deconvolved CCD Hα image with the Lucy-Richardson algorithm taking as a point spread function the response of a field star and having only 1 iteration. Some benefits of this algorithm are that it is fast, preserves details of different structures with different angular sizes and does not explicity uses the point spread function of the total telescope system (that could be different from night to night). Details of the polynomial transform algorithm applied to astronomical images and a comparison with other algorithms will be published elsewhere. The I and Hα images presented here have been deconvolved with the polynomial transform algorithm.

2.3. Hα Spatial Distribution

In discussing the nuclear emission of spiral galaxies, one has to be aware of the meaning of the term. Prior to the *Hubble Space Telescope* high resolution observations, the emission coming from the innermost 5″ was usually called "nuclear emission". With the recent *HST* high resolution observations of barred galaxies (see, for example, Wilson et al.

1993) one can resolve several components within the central 5″. Thus the old term includes both the compact nucleus at the kinematical center and some of the innermost circumnuclear regions. Our observations have a resolution better than 1.5″ but, unless one component is clearly missing, we cannot differentiate the circumnuclear emission from the one of the compact nucleus. To avoid any possible confusion, we simply use the term "innermost central region" for the emitting regions at or near the center.

The CCD images of the ionized gas in 51 galaxies were done with the narrowband filter Hα. For one galaxy, NGC 672, we only have a broadband image. For simplicity, the results are organized according to the spatial distribution of the emission. The regions considered are: 1) the *innermost central regions* —i.e., inside the central 5″—, 2) *circumnuclear structures* or nuclear rings, 3) the stellar *bar*, 4) the *ends of the bar*, 5) *inner rings* just outside the bar, 6) normal H II regions from the *disk*, 7) *outer* rings, and 8) emission *perpendicular* either to the stellar bar or to the normal spiral arms. The images have not been flux calibrated and they have not been corrected for extinction. We have used contour maps and false color image techniques of the deconvolved Hα images in order to determine the location of the emission with the best relative signal to noise ratio in each of them. Figures 2 to 48 show the I and Hα images of the observed sample. The Hα morphology for the 51 *barred* galaxies is listed in Table 4.

TABLE 4

Hα SPATIAL DISTRIBUTION

NGC/IC	Compact Nucleus	Disk H II	Nuclear Ring	Inner Ring	Outer Ring	Along Bar	Ends of Bar	Perp.[a] to Arms	Pec[b] Morph.
N 672	...	...	...	...	...	...	...	...	...
N 1022	Y	...	...	...	...	...	...	Y	...
N 1326	...	...	Y	...	...	...	...	...	...
I 1953	Y	Y	...	...	...	...	...	...	...
N 1415	...	...	Y	...	...	...	Y	...	...
N 1637	Y	Y	...	...	...	...	...	...	...
N 1784	Y	Y	...	Y	...	...	...	...	...
N 1832	Y	...	...	Y	...	...	...	...	...
N 2139	...	Y	...	...	...	Y	...	Y	...
N 2217	...	...	...	...	Y	...	...	...	...
N 2223	...	Y	...	Y	...	...	...	...	...
N 2339	Y	Y	...	...	...	...	...	Y	...
N 2525	Y	Y	...	...	...	...	Y	...	Y[c]
N 2545	...	...	...	Y	...	...	...	Y	...
N 2798	Y	Y	...	...	...	...	...	...	...
N 2787	...	...	...	...	...	...	...	...	...
N 2835	...	Y	...	...	...	Y	...	...	...
N 3185	Y	Y	...	Y	...	...	...	...	...

TABLE 4 (CONTINUED)

NGC/IC	Compact Nucleus	Disk H II	Nuclear Ring	Inner Ring	Outer Ring	Along Bar	Ends of Bar	Perp.[a] to Arms	Pec.[b] Morph.
N 3287	Y	Y	...	...	...	Y	...	...	...
N 3318	Y?	Y	Y?	...	...	Y	Y	...	...
N 3319	...	Y	...	...	...	...	Y	Y	...
N 3351	...	Y	Y	Y	Y	...	...	...	...
N 3359	...	Y	...	...	...	Y	Y	...	...
N 3367	Y	Y	...	...	...	...	...	...	Y[d]
N 3504	Y	Y	...	Y	...	Y	Y	...	...
N 3513	...	Y	...	...	...	...	Y	Y	...
N 3783	Y	...	...	Y	...	...	...	Y	Y[e]
N 3912	Y	Y	...	...	...	Y	...	...	...
N 4123	Y	Y	...	...	...	Y	Y	...	...
N 4314	...	...	Y	...	...	...	...	...	...
N 4385	Y	...	...	...	...	Y	Y	...	...
N 4435	...	...	...	...	...	...	...	...	...
N 4477	...	...	...	...	...	...	...	...	...
N 4507	Y	...	...	Y	...	...	...	...	...
N 4561	Y	Y	...	...	...	Y	Y	...	...
N 4688	...	...	...	...	Y	...	...	...	...
N 4691	...	...	...	...	...	Y	...	...	Y[f]
N 5135	Y	...	Y	...	...	...	Y	...	...
N 5188	Y	...	...	...	...	...	...	...	...
N 5347	Y	...	Y	...	...	Y	...	...	...
N 5430	...	Y	Y	...	...	Y	Y	...	...
N 5534	Y	...	...	...	...	...	Y	...	...
N 5597	Y	...	...	...	...	Y	Y?	...	...
N 5691	...	...	...	...	...	Y	Y	...	...
N 5728	Y[g]	...	Y	...	...	...	Y	Y	...
N 5757	Y	Y	...	...	...	Y	Y	...	...
N 5915	...	Y	...	...	...	...	...	Y	...
N 6239	Y	Y	...	...	...	Y	...	...	...
N 6907	Y	...	...	...	...	Y	Y	...	...
N 6951	Y	...	Y	...	...	...	...	...	...
I 5273	Y	...	...	...	...	...	Y	...	...
N 7479	Y?	Y	...	...	...	Y	...	...	...

[a] Hα perpendicular to normal spiral arms or along the minor axis of bars.

[b] Hα peculiar morphology.

[c] NGC 2525 has a two parallel spiral arms to the SE.

[d] NGC 3367 shows a string of Hα emission along the outermost SW edge of the galaxy forming a semicircular structure.

[e] NGC 3783 has Hα emission in a direction along the minor axis of the bar and possibly extending to the SW (see also Forte et al. 1987; Winge et al. 1992).

[f] NGC 4691 shows Hα emission mainly from four bright sources in dense environments in the central part of the galaxy (García-Barreto et al. 1995).

[g] Higher angular resolution Hα images and spectroscopy suggest that Hα is minimum at the kinematical center or compact nucleus (Arribas & Mediavilla 1993).

Thirty-two galaxies (63%) present Hα emission from the innermost central regions. Ten galaxies (20%) show circumnuclear Hα emission that could be ascribed to nuclear rings. Eighteen galaxies (35%) present Hα from regions along the bar and 10 out of these 18 show also nuclear Hα emission. Eighteen galaxies (35%) show Hα emission from the ends of the stellar bar. Nine (17%) show emission from inner rings, that is, structures just outside the stellar bar. Twenty-six galaxies (50%) show Hα emission
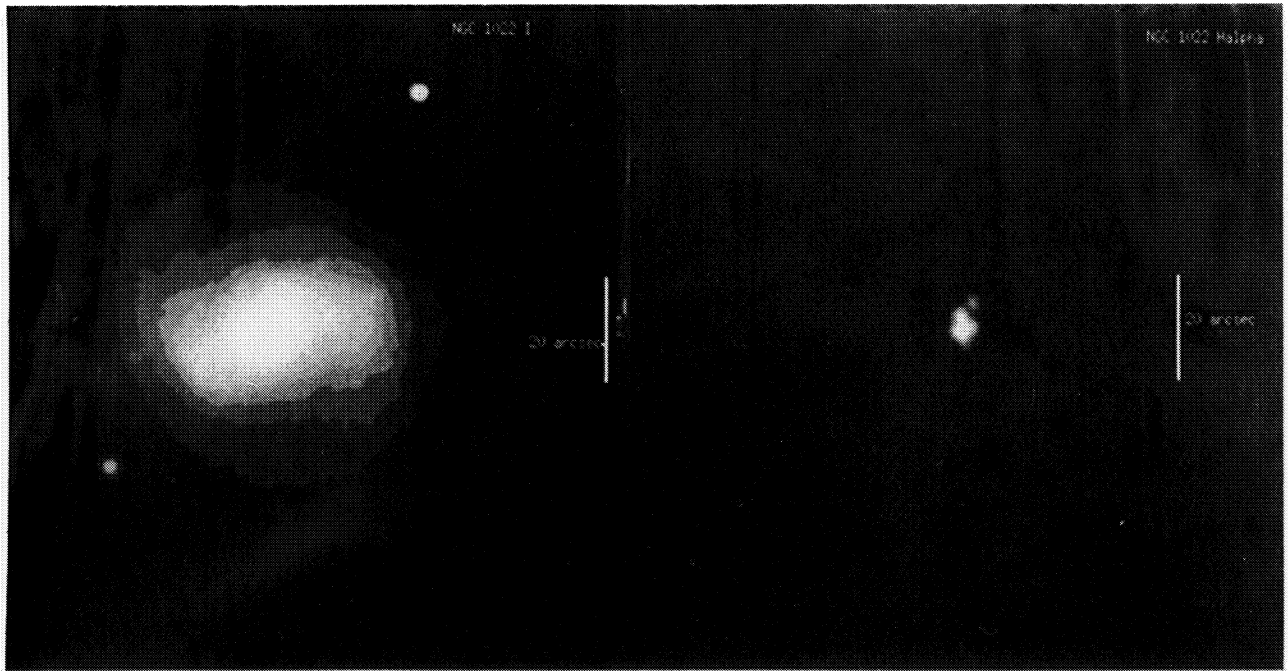
Fig. 2. *I* and Hα images of NGC 1022. The vertical scale is 20″, north is up, east is left.
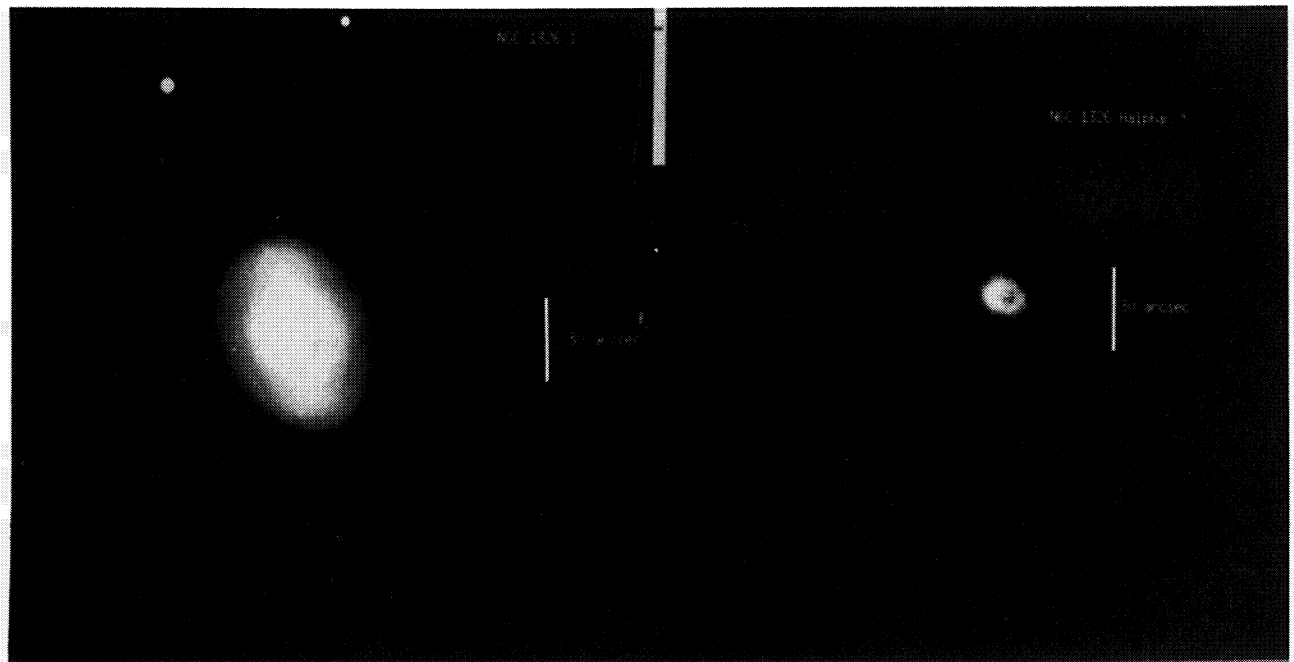
Fig. 3. *I* and Hα images NGC 1326. The vertical scale is 30″, north is up, east is left.
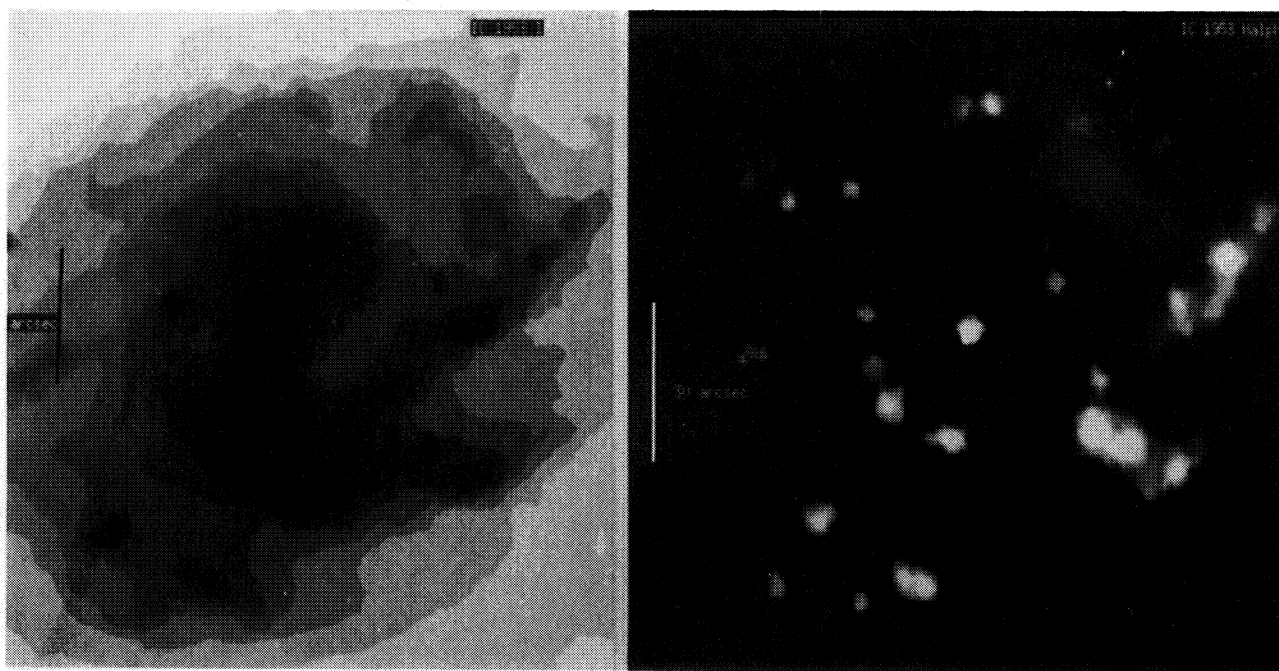
Fig. 4. I and Hα images of IC 1953. The vertical scale is $30''$, north is up, east is left.
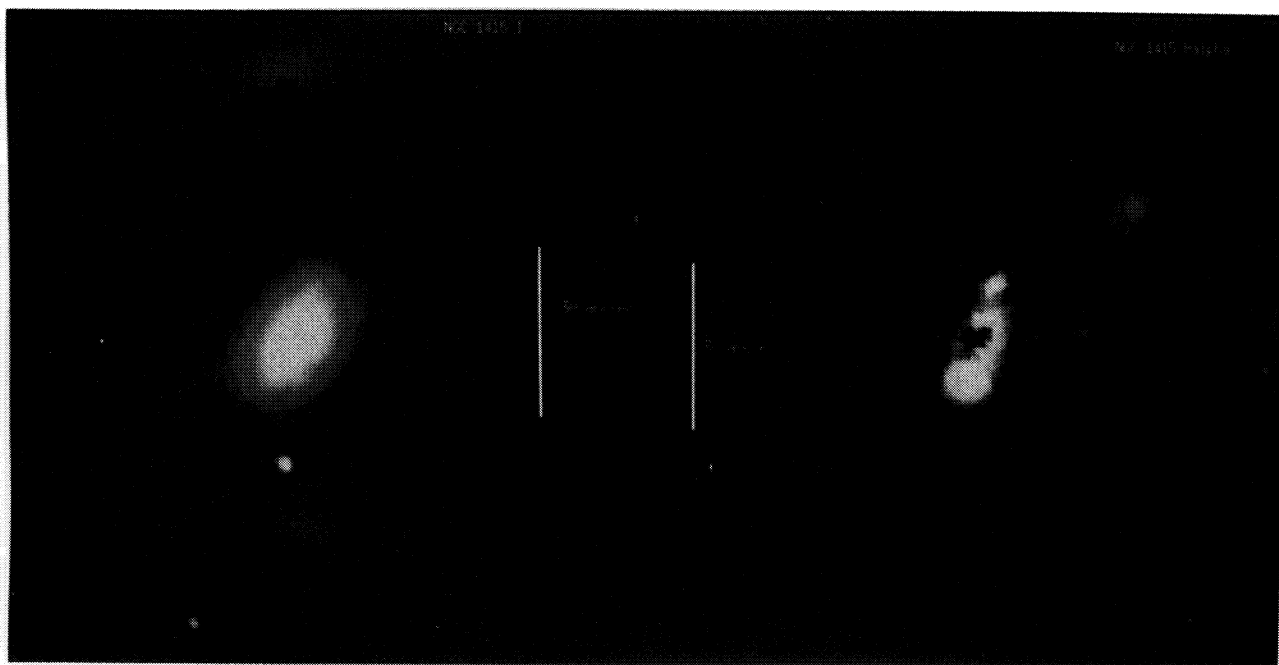
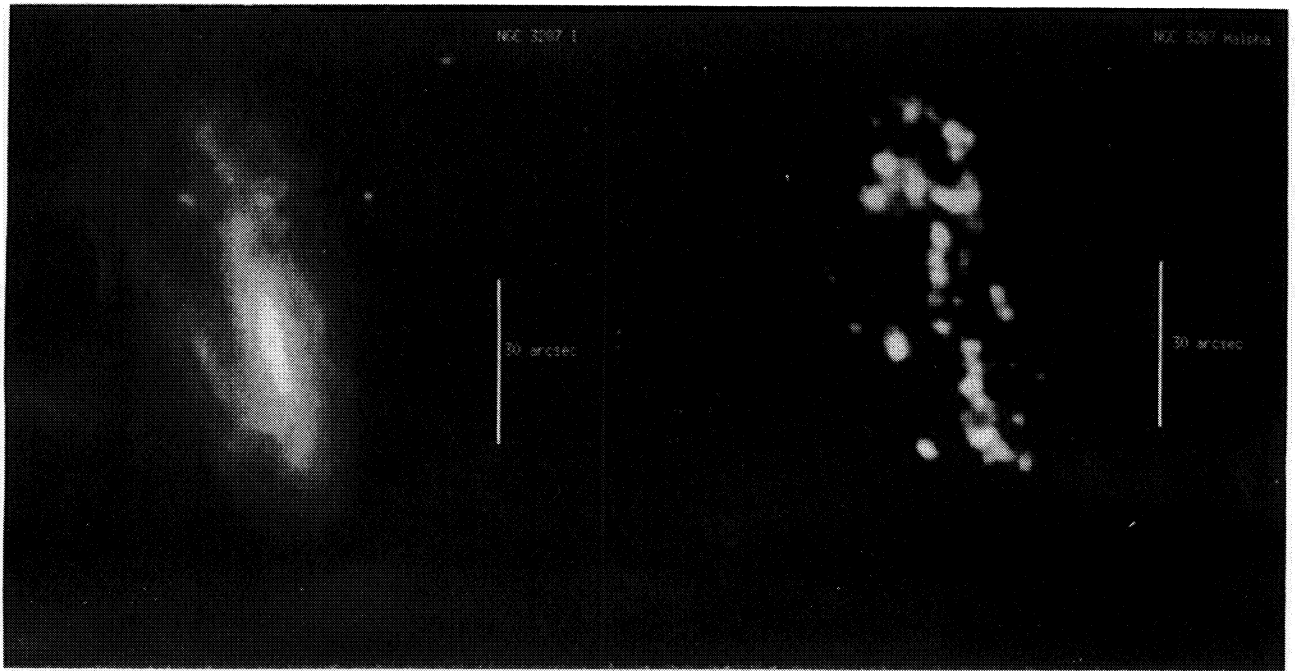Fig. 5. I and Hα images of NGC 1415. The vertical scale is $30''$, north is up, east is left.
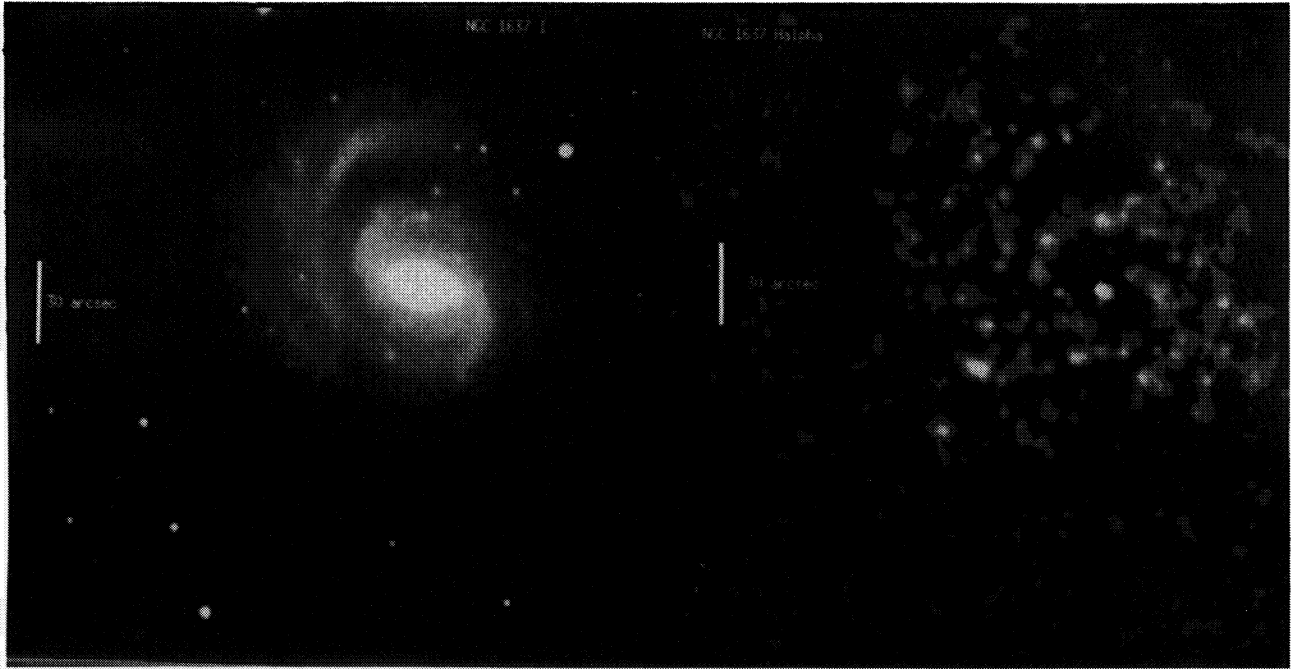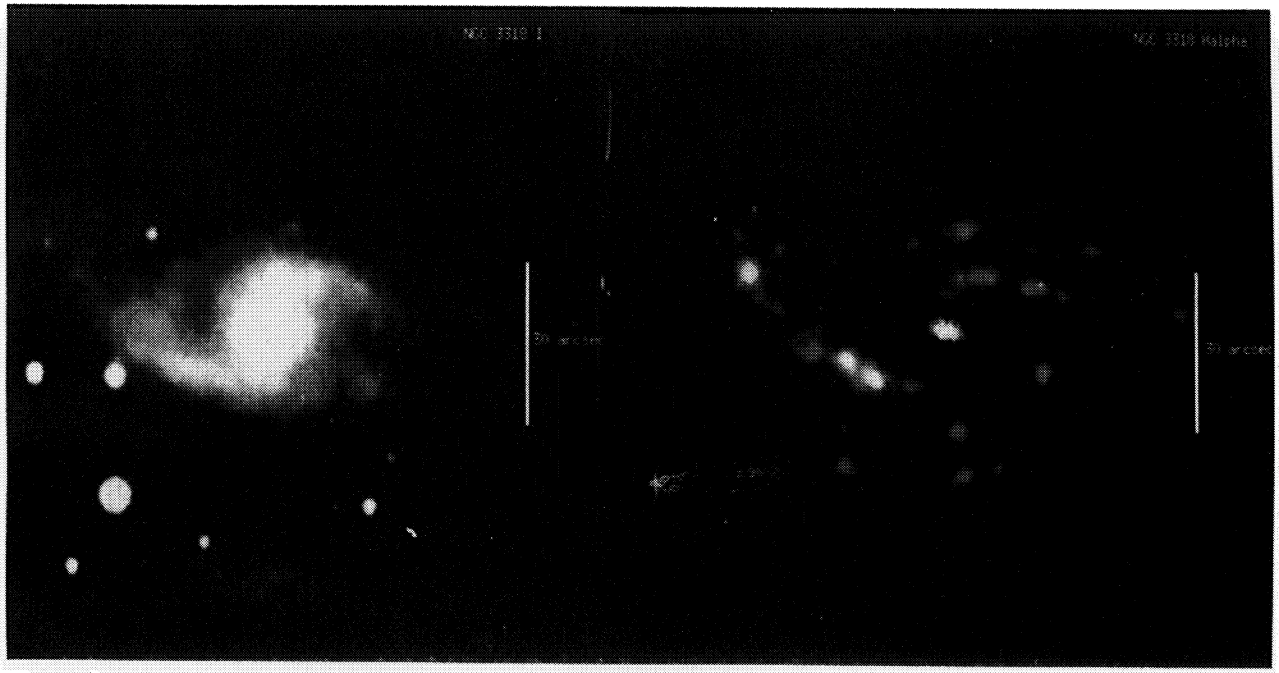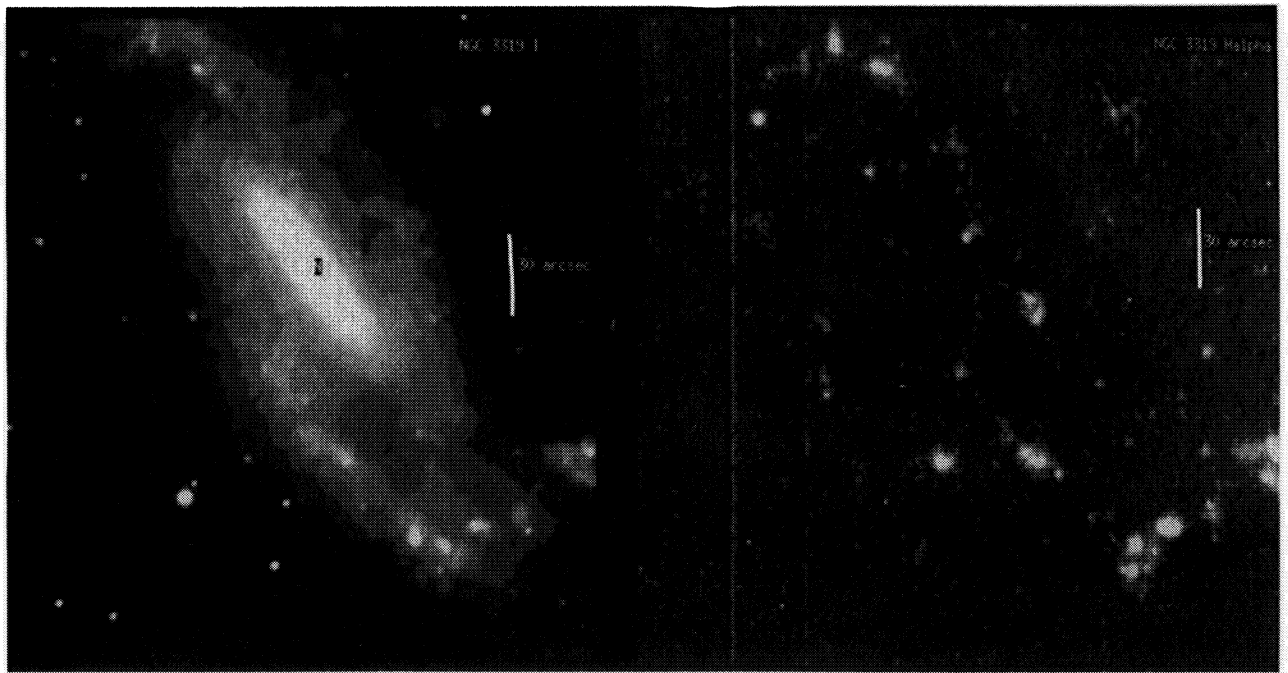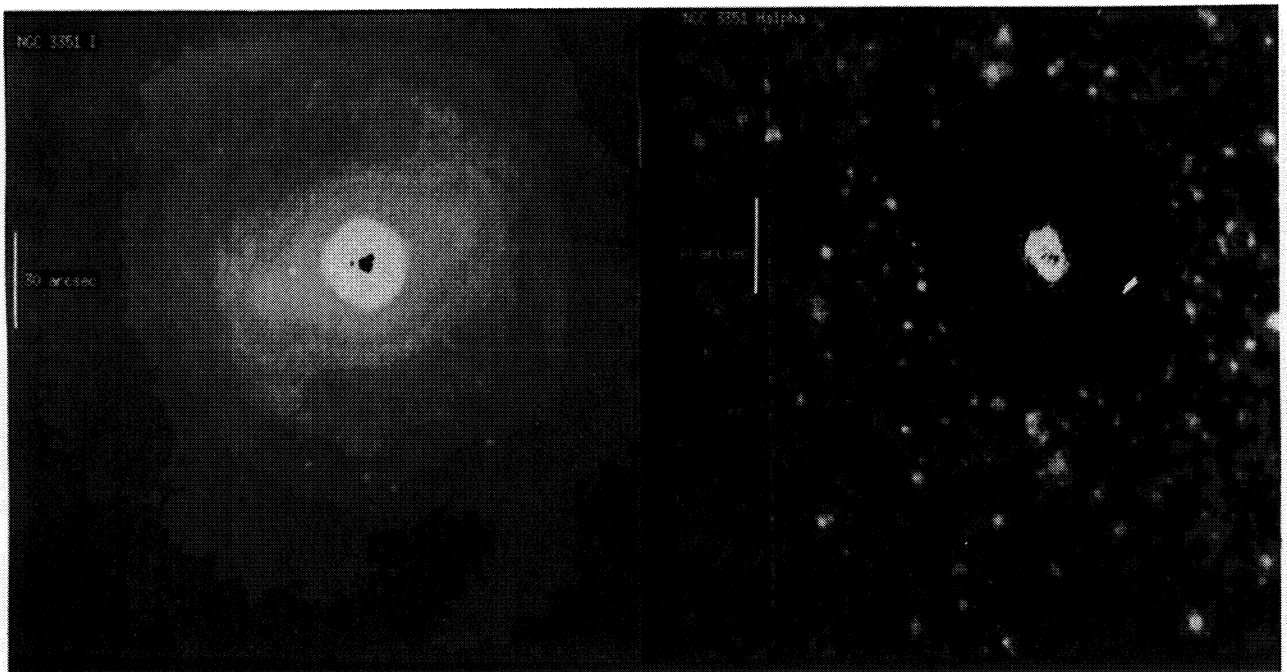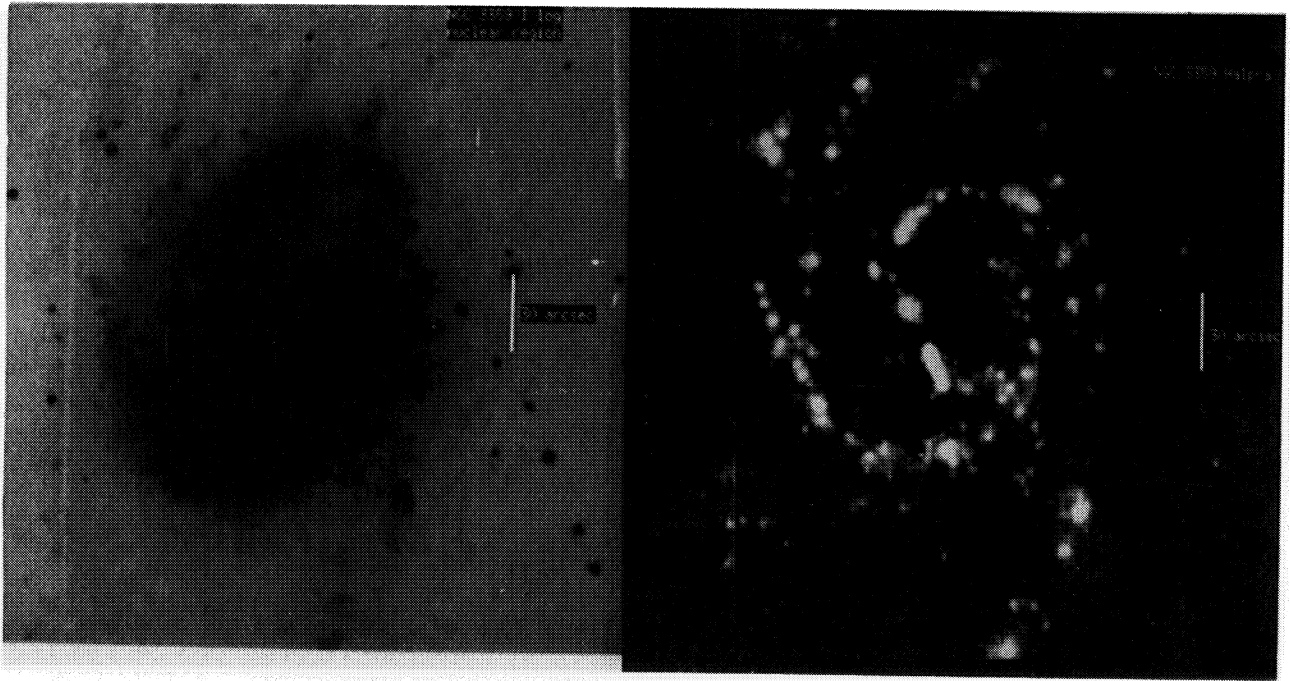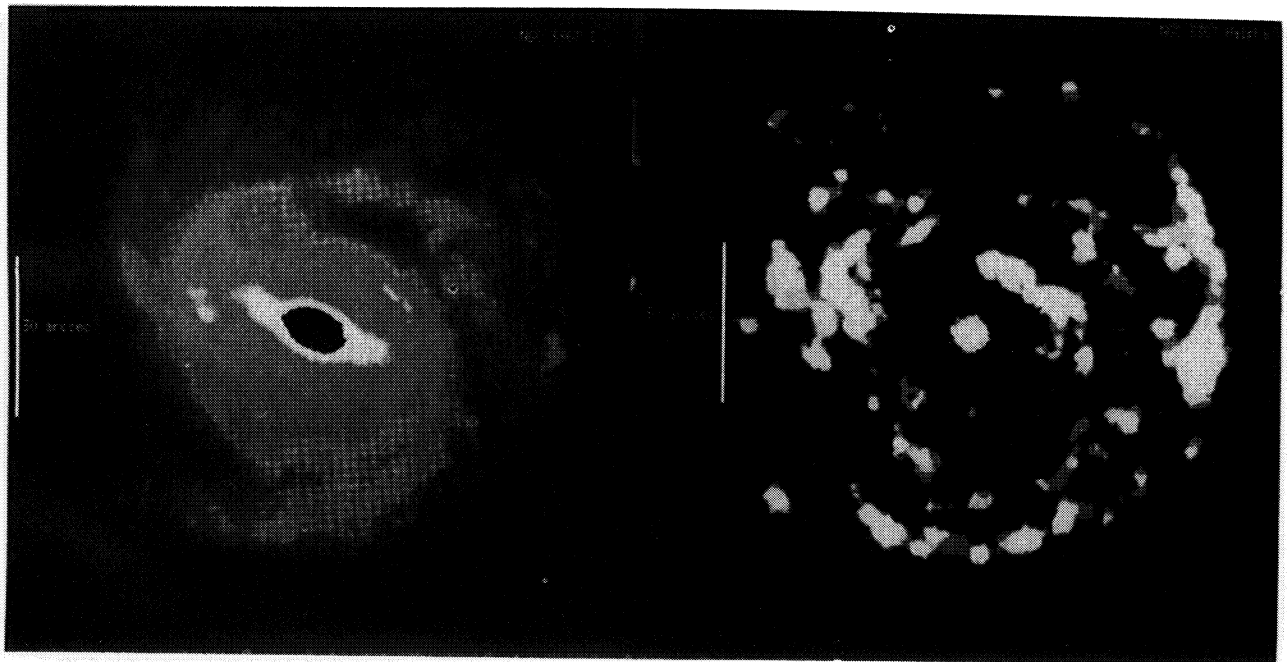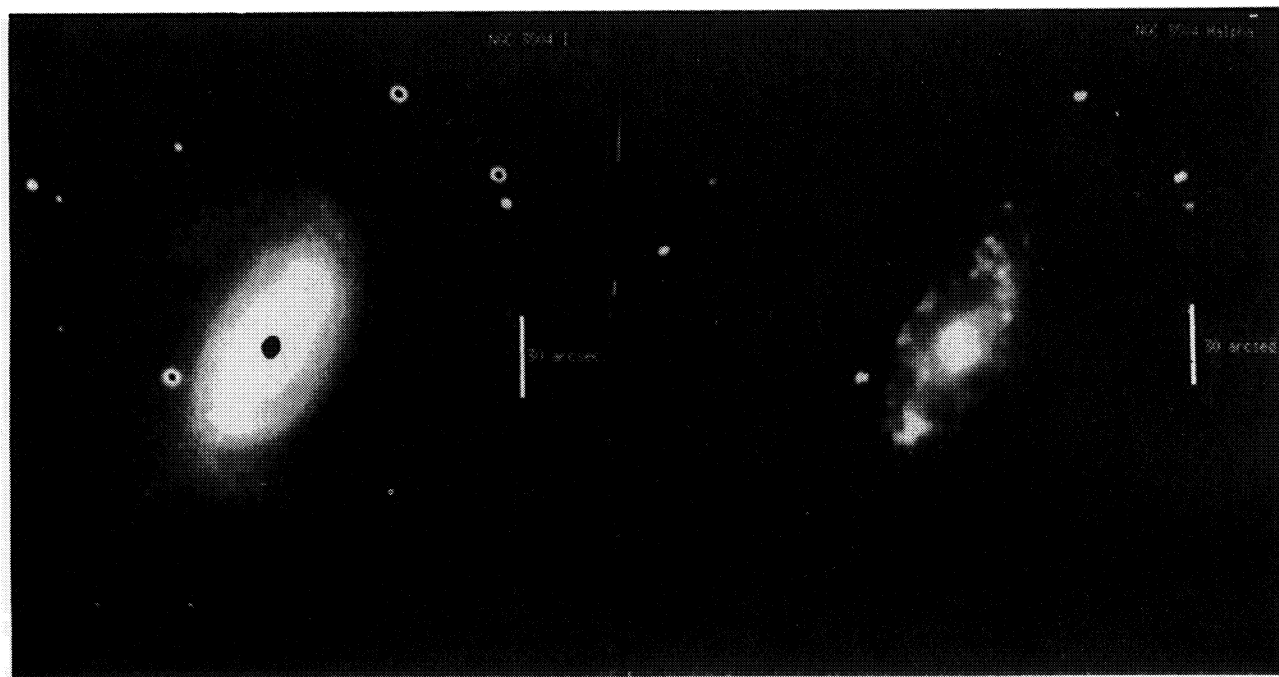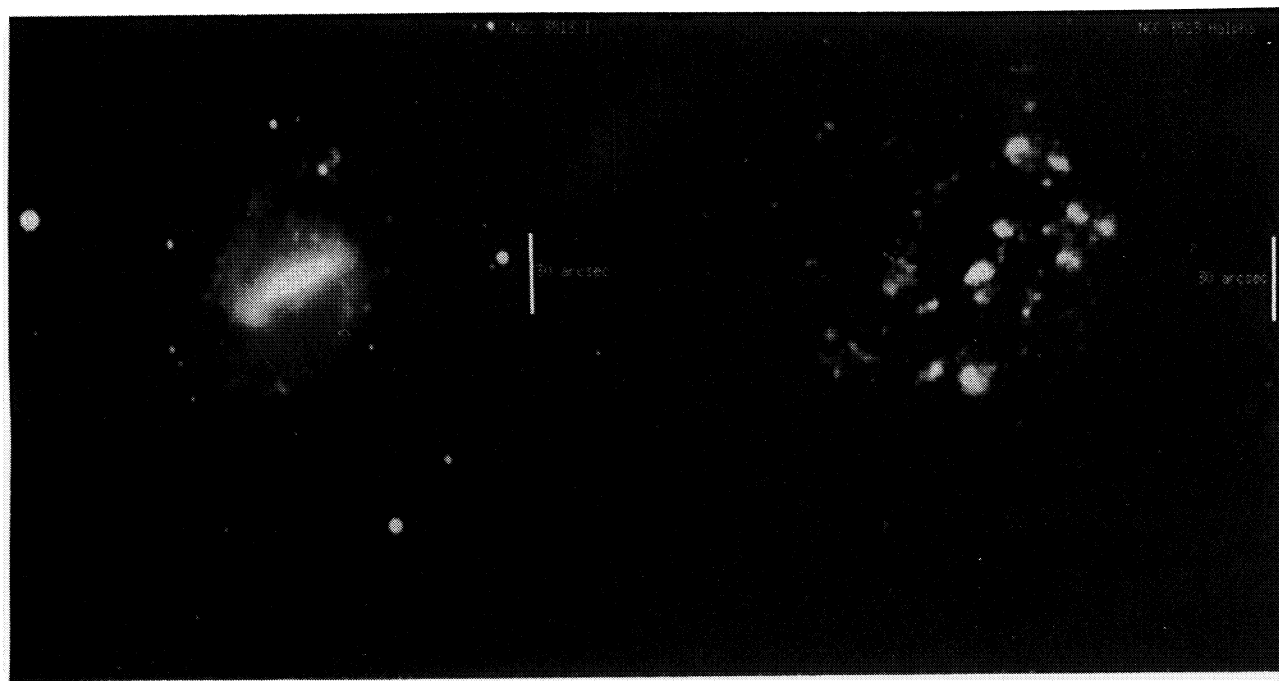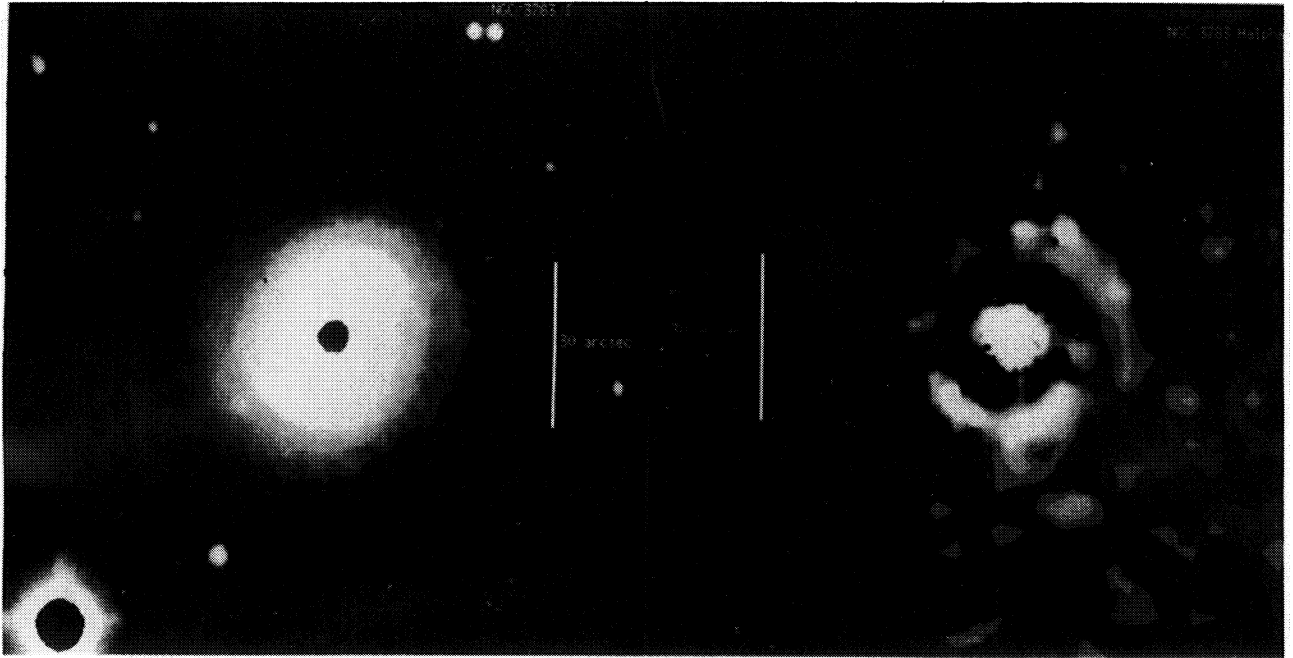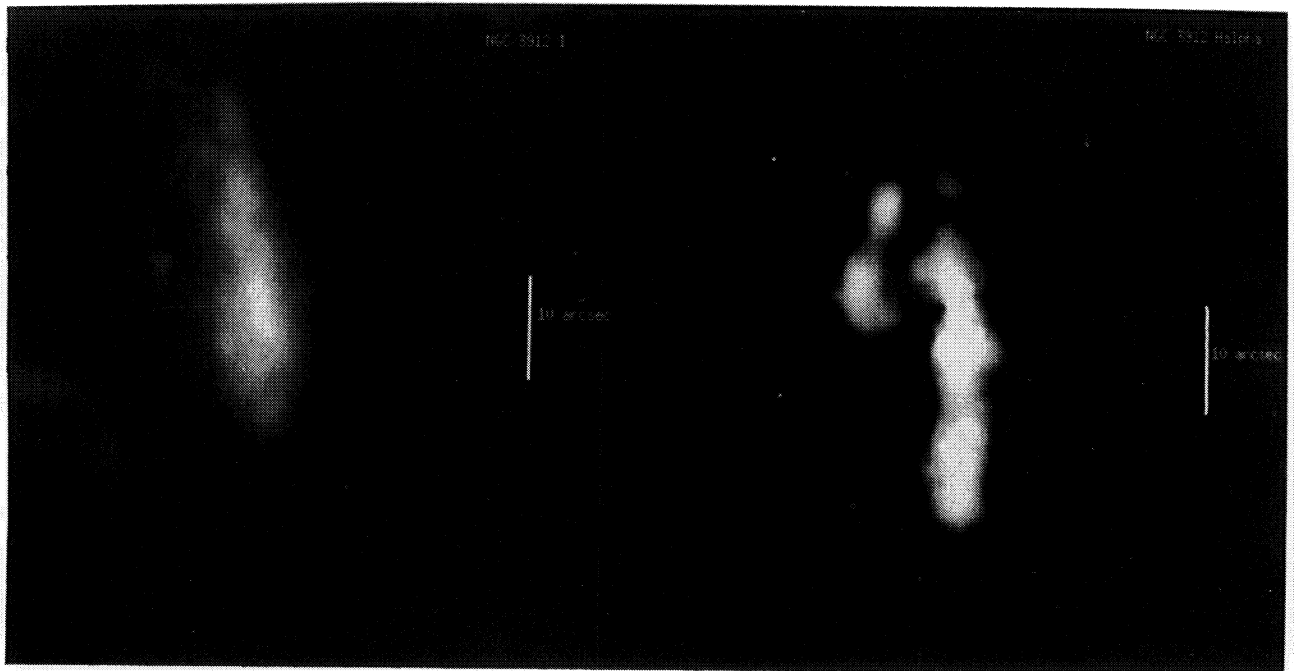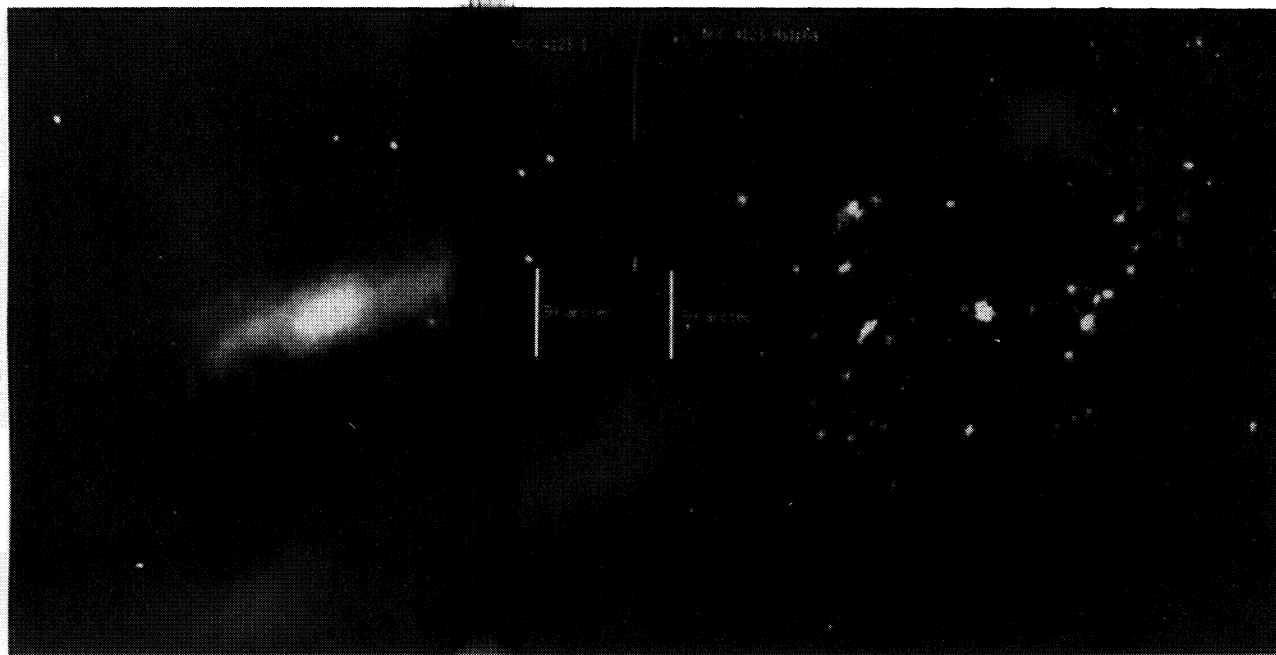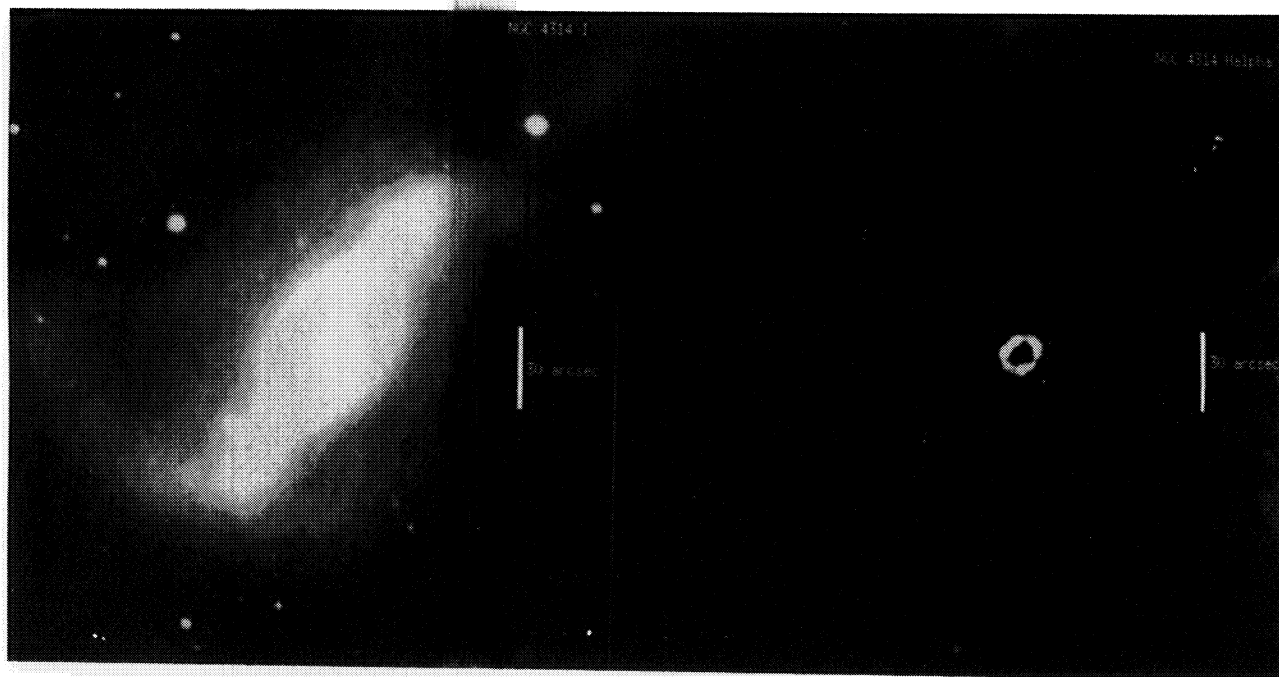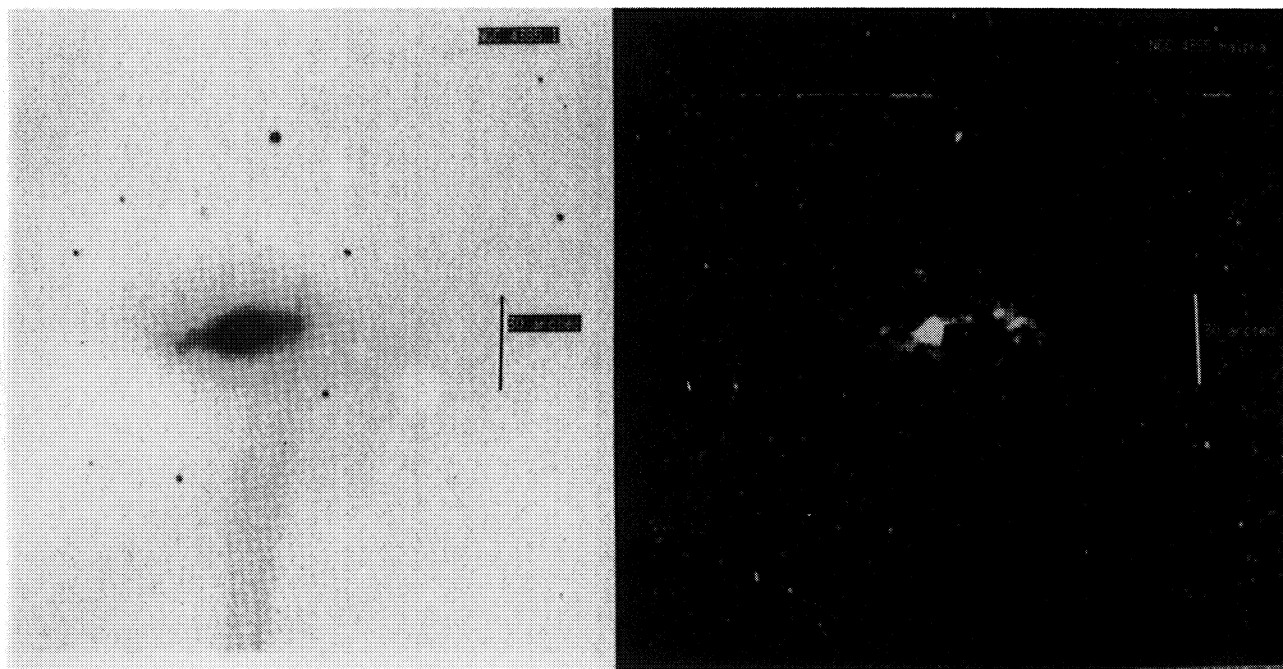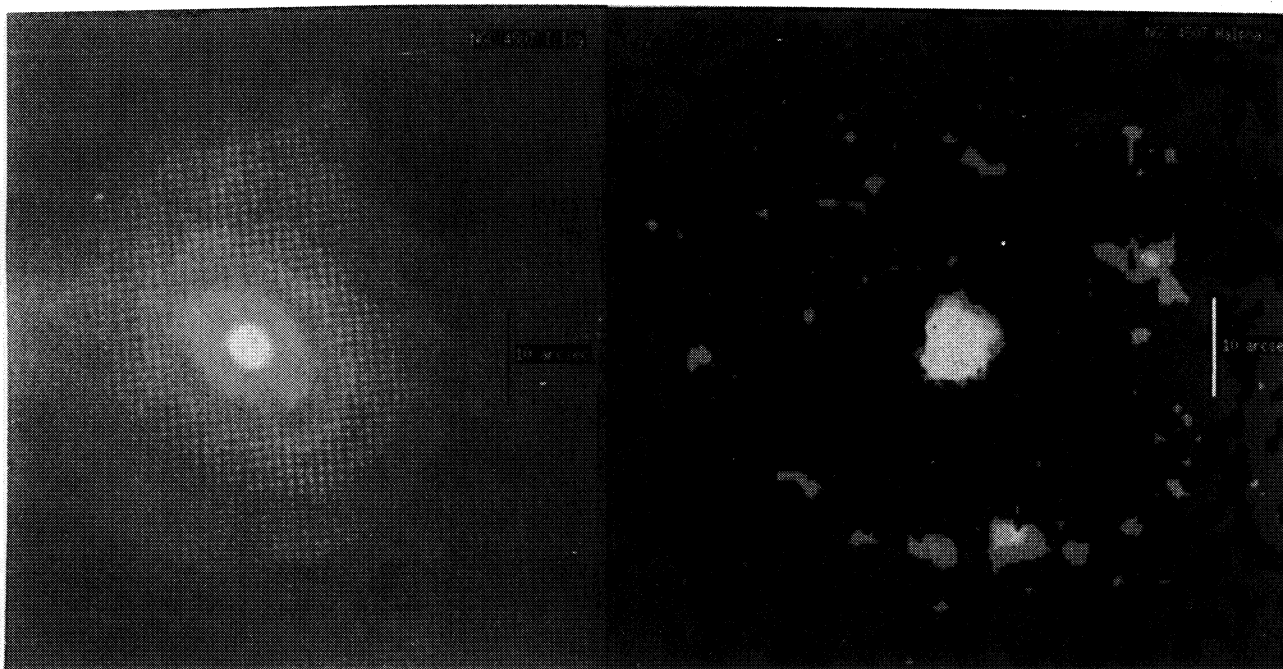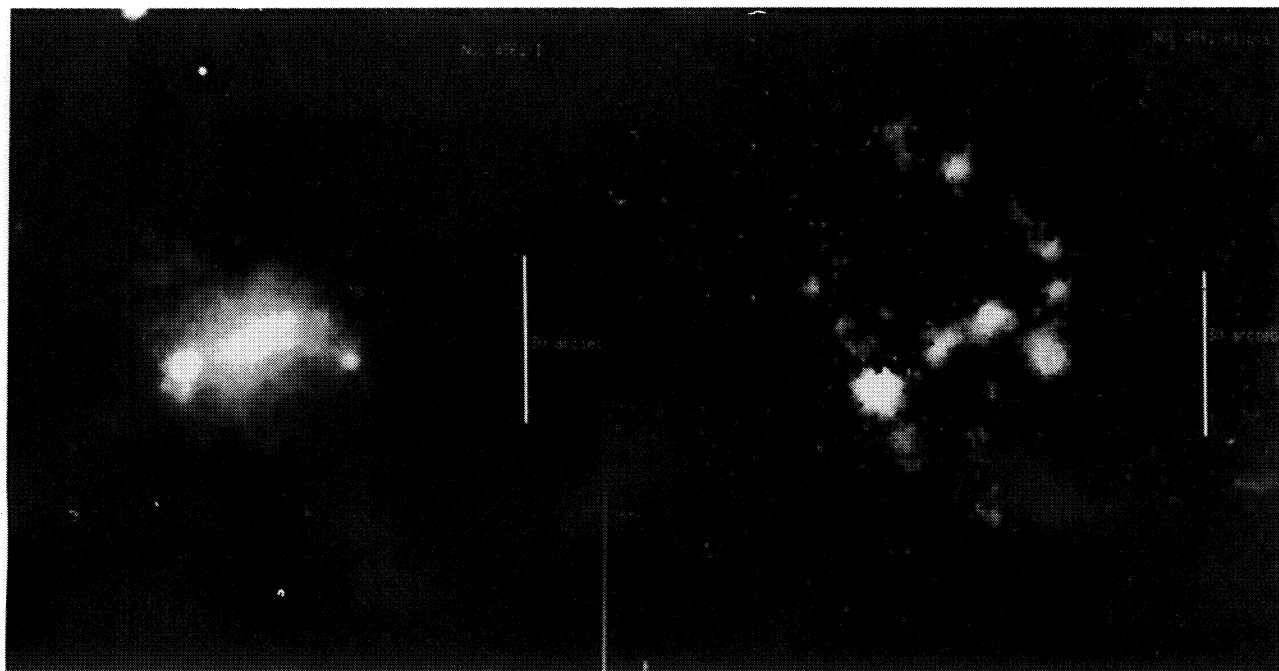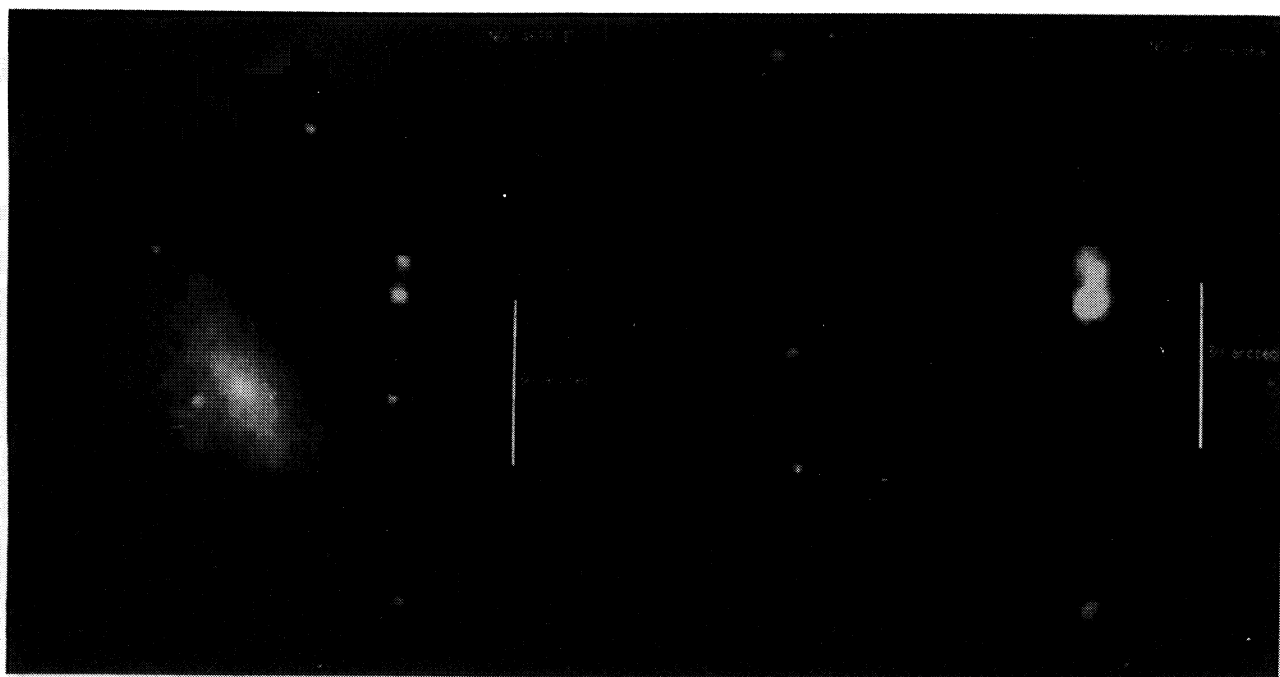
Fig. 6. I and Hα images of NGC 1637. The vertical scale is 30″, north is up, east is left.
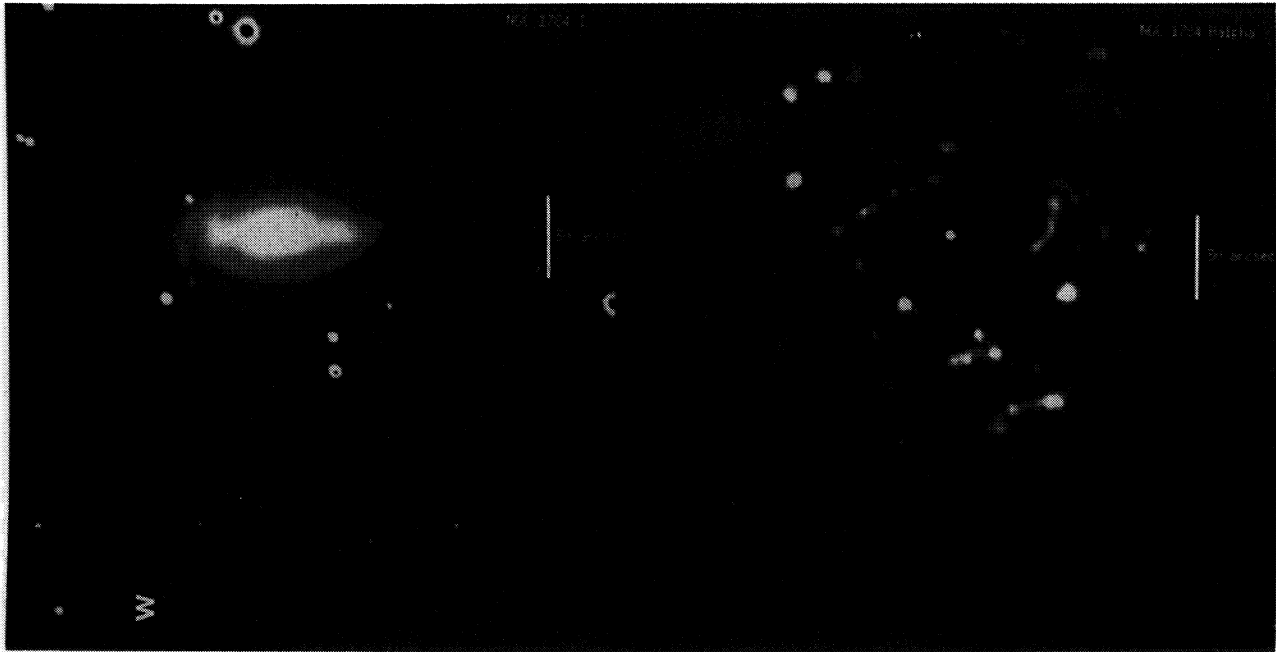
Fig. 7. I and Hα images NGC 1784. The vertical scale is 30″, north is up, east is left.

GARCÍA-BARRETO ET AL.
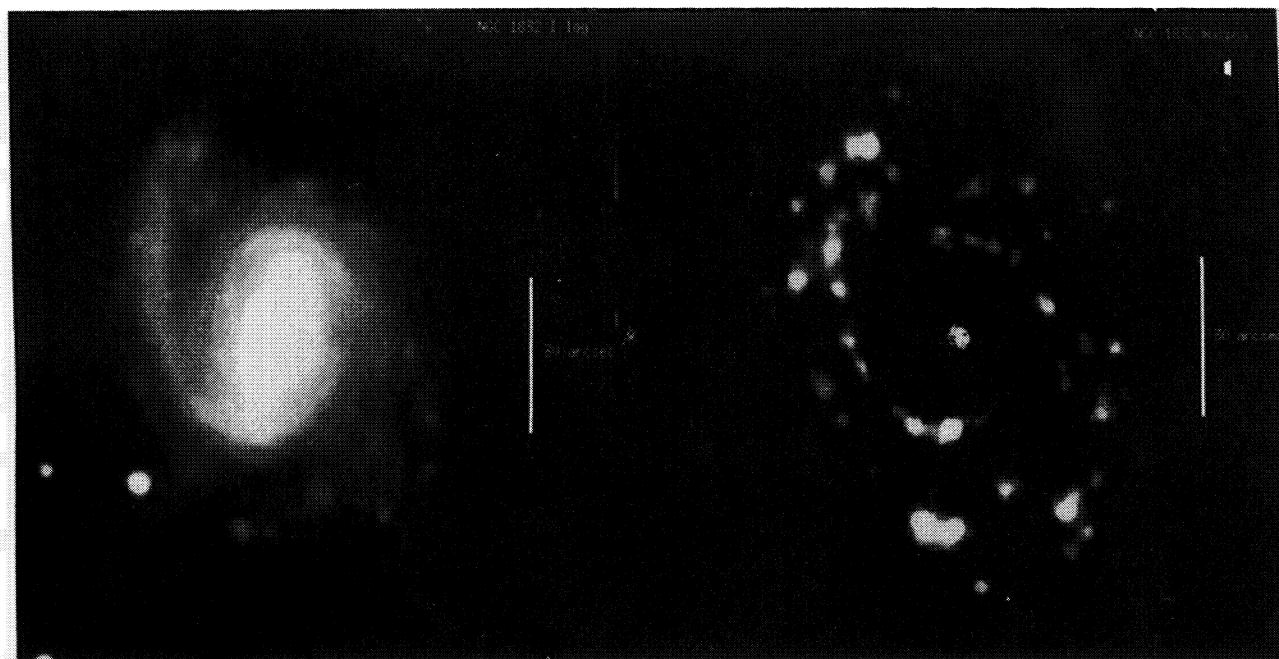
Fig. 8. *I* and Hα images of NGC 1832. The vertical scale is 30″, north is up, east is left.
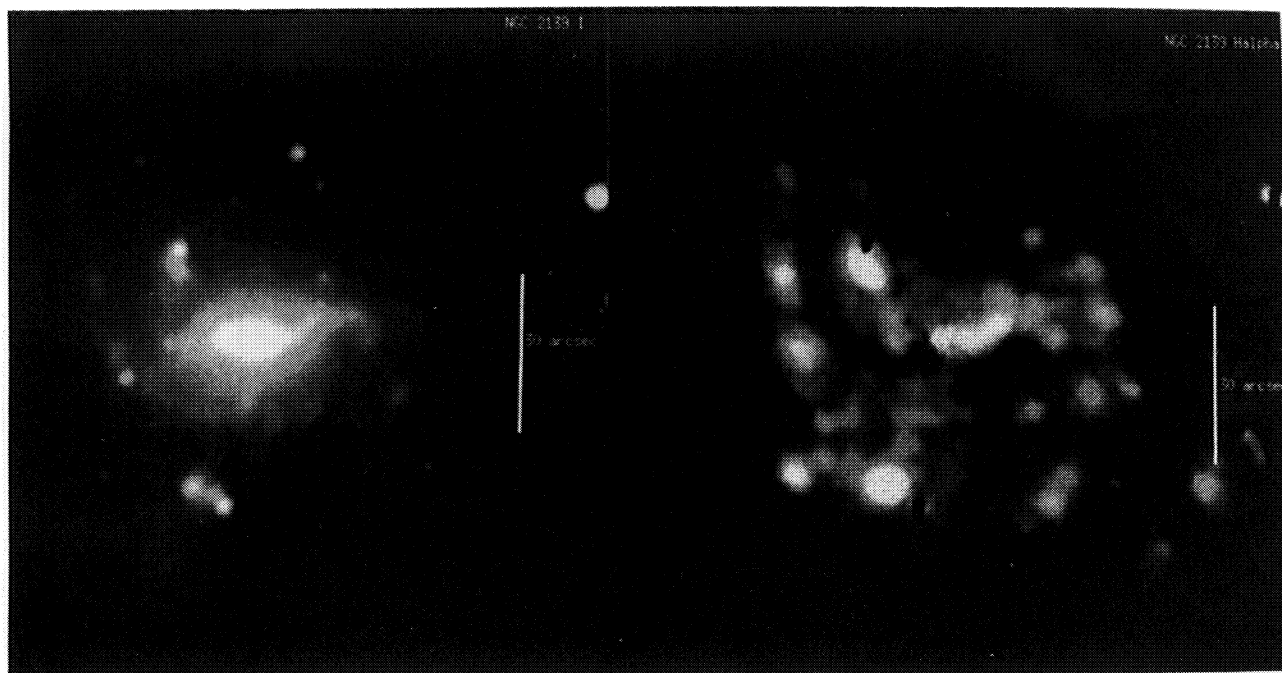
Fig. 9. *I* and Hα images of NGC 2139. The vertical scale is 30″, north is up, east is left.
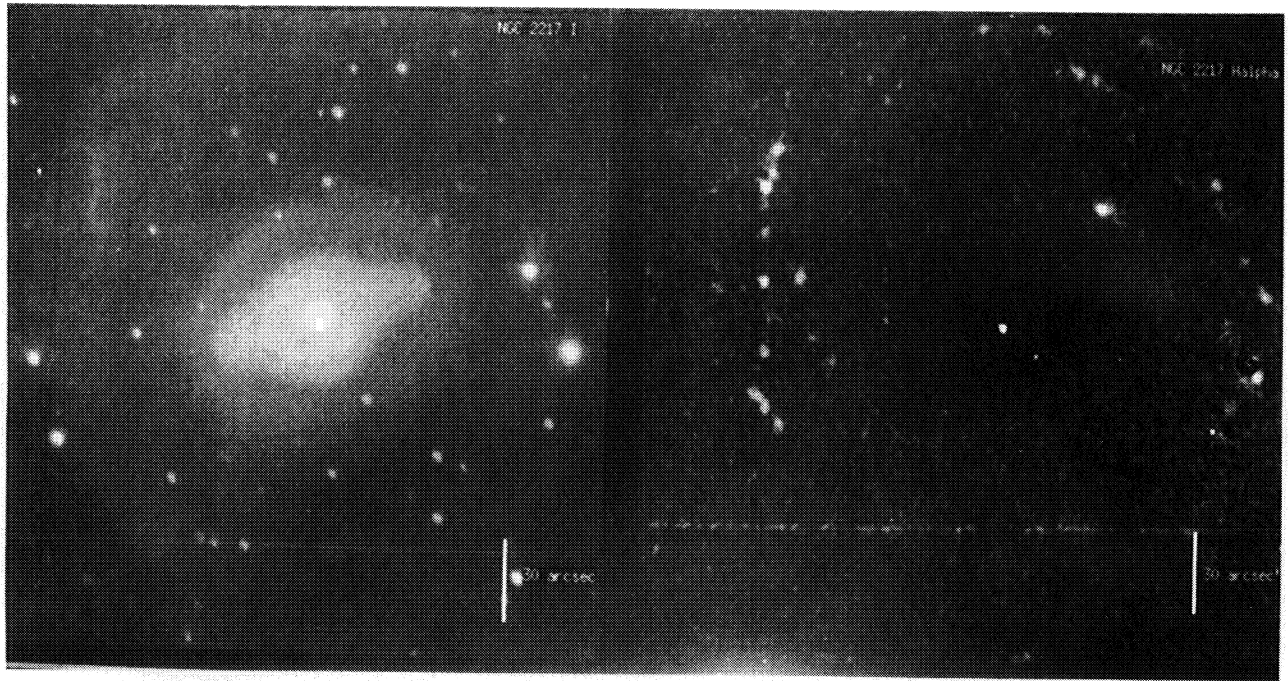
Fig. 10. I and Hα images of NGC 2217. The vertical scale is $30''$, north is up, east is left.
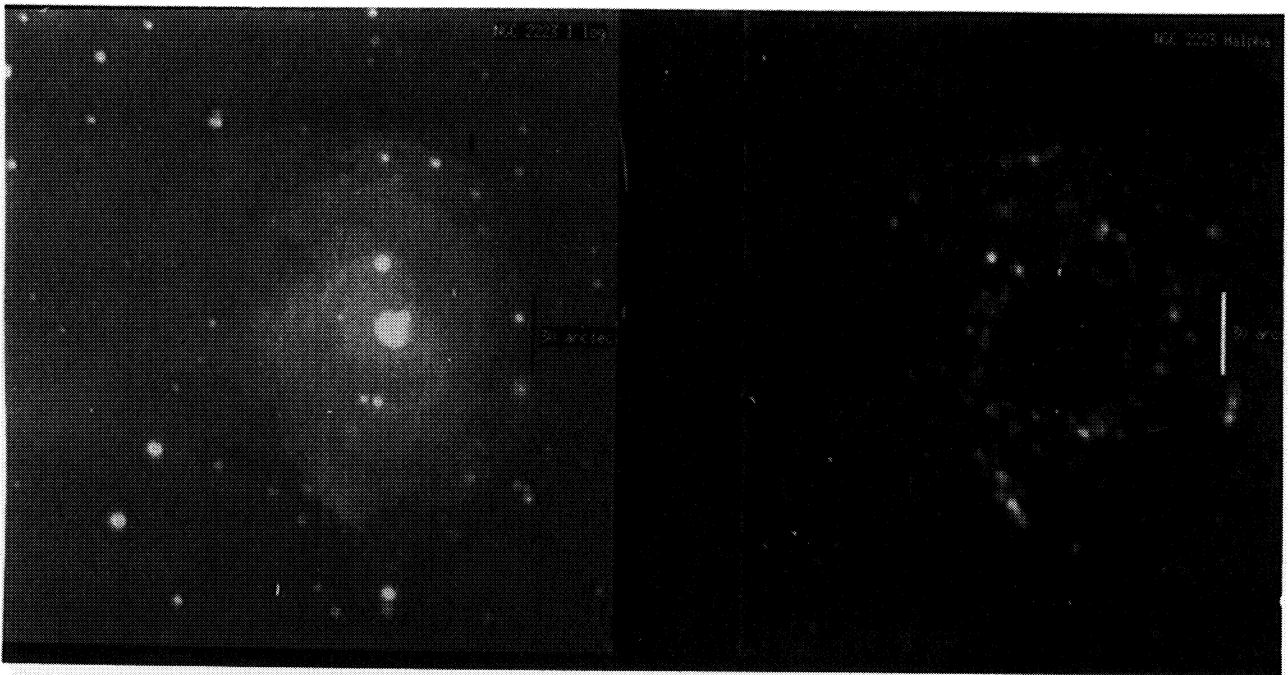
Fig. 11 I and Hα images of NGC 2223. The vertical scale is $30''$, north is up, east is left.
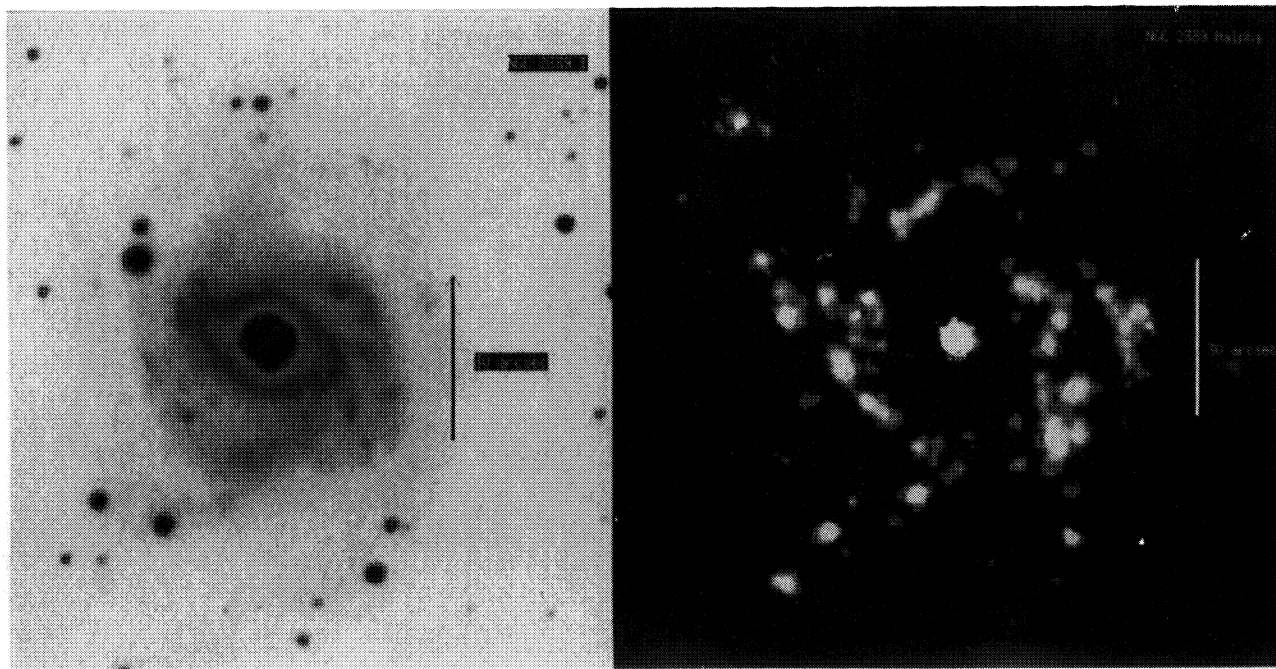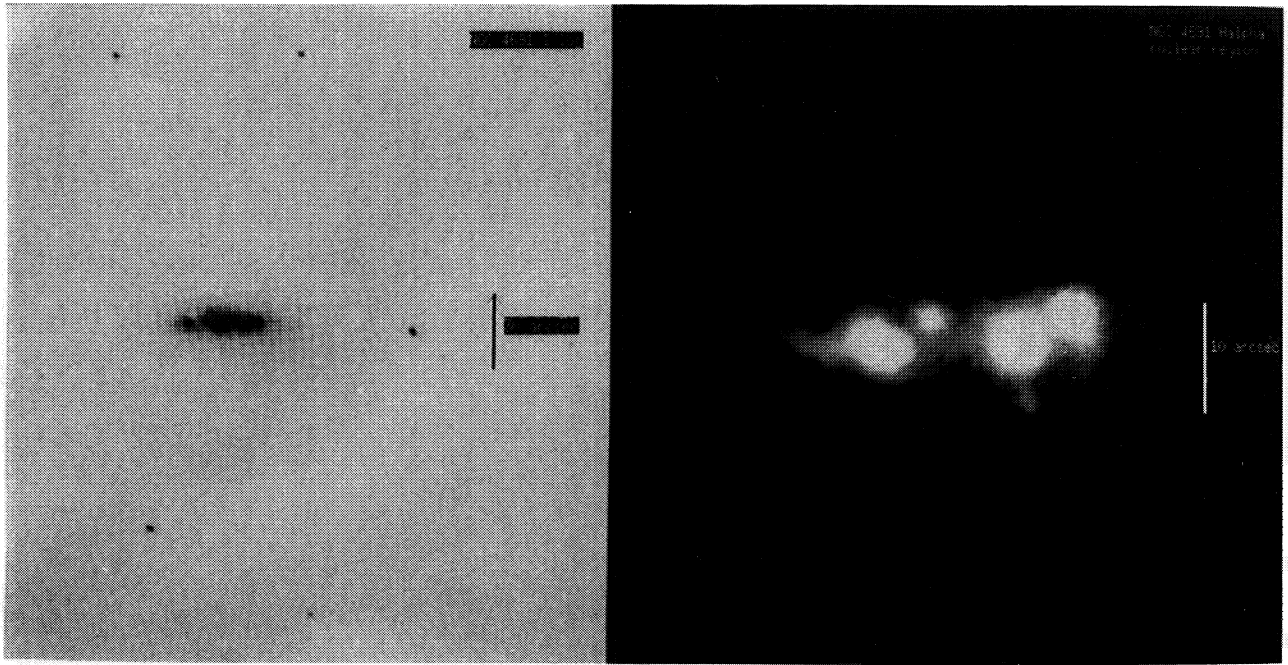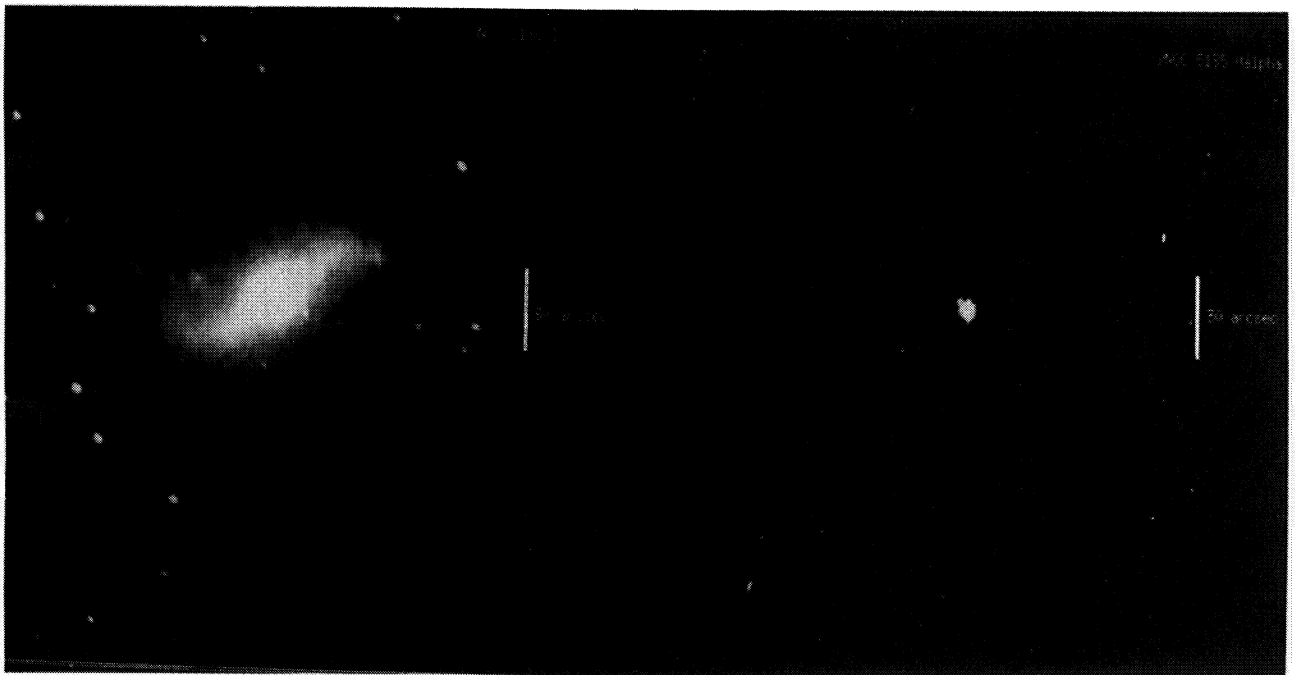
Fig. 12. I and Hα images of NGC 2339. The vertical scale is 30$''$, north is up, east is left.
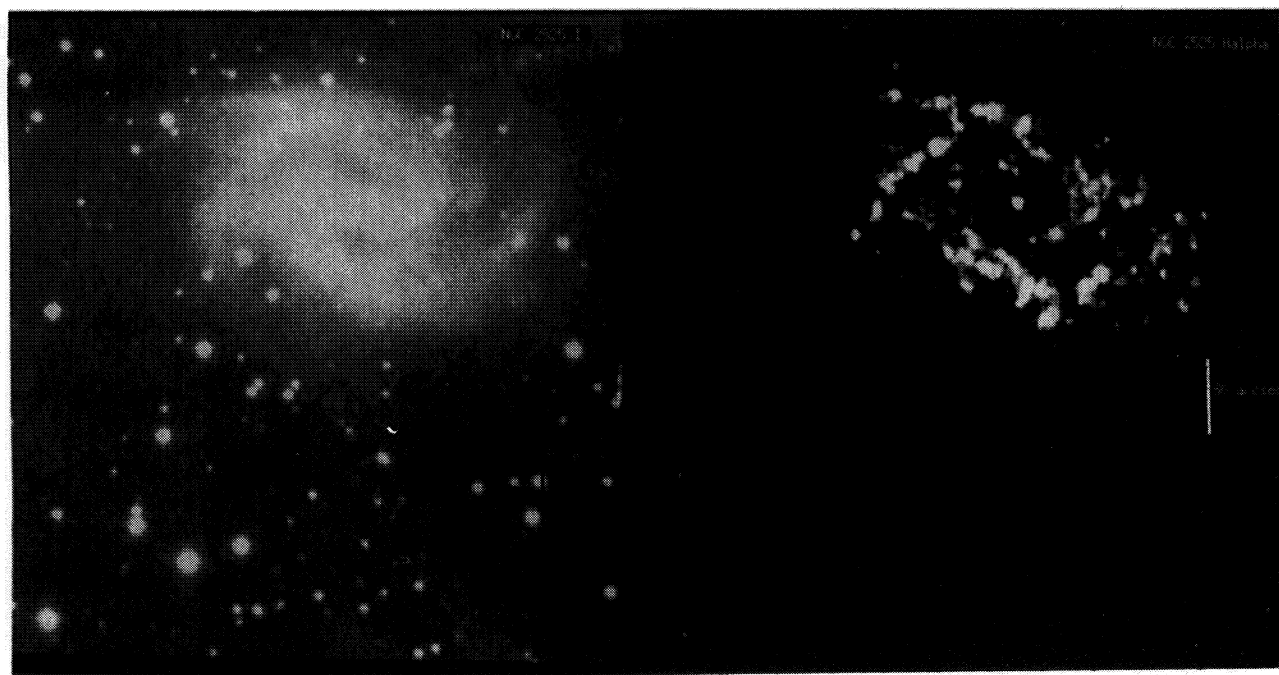
Fig. 13. I and Hα images of NGC 2525. The vertical scale is 30$''$, north is up, east is left.
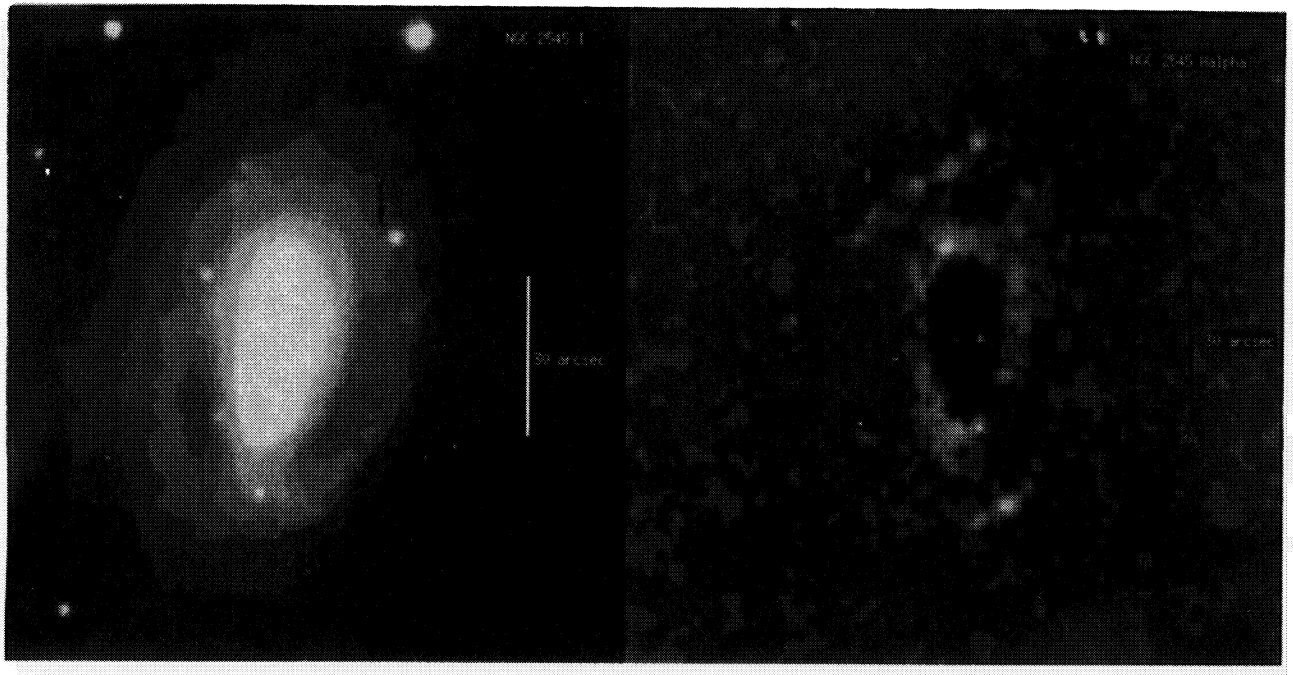
Fig. 14. *I* and Hα images of NGC 2545. The vertical scale is 30″, north is up, east is left.
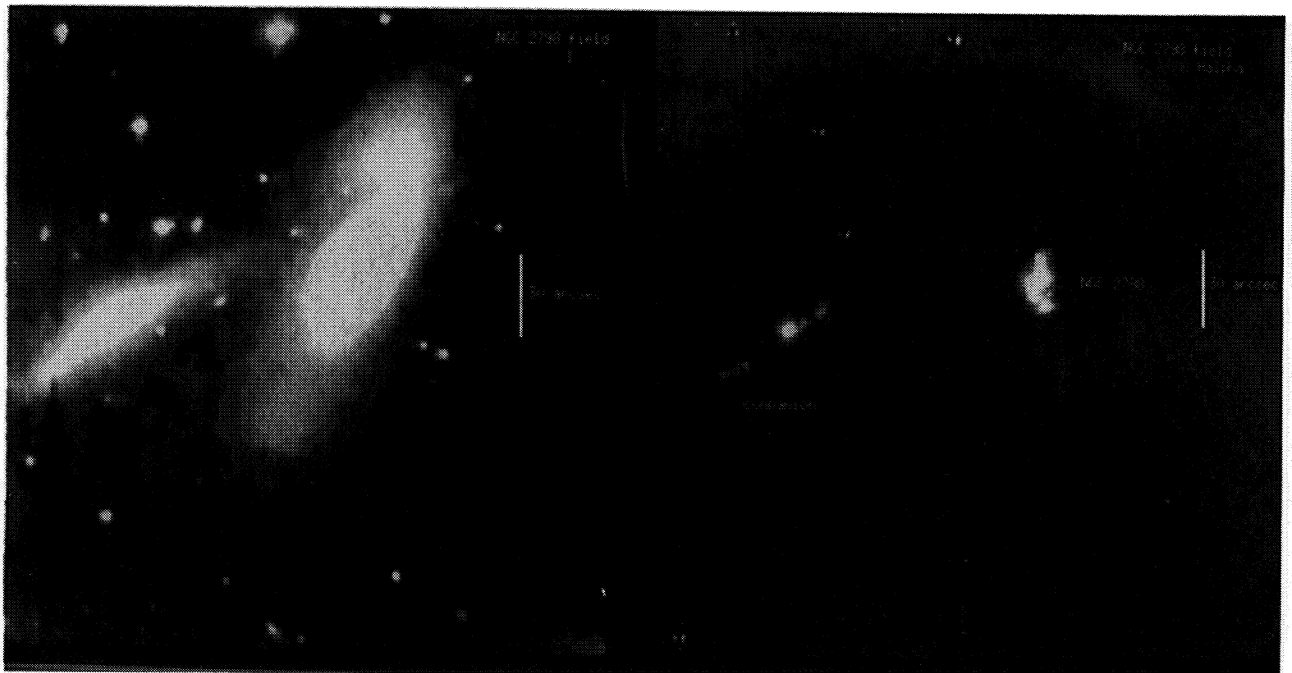
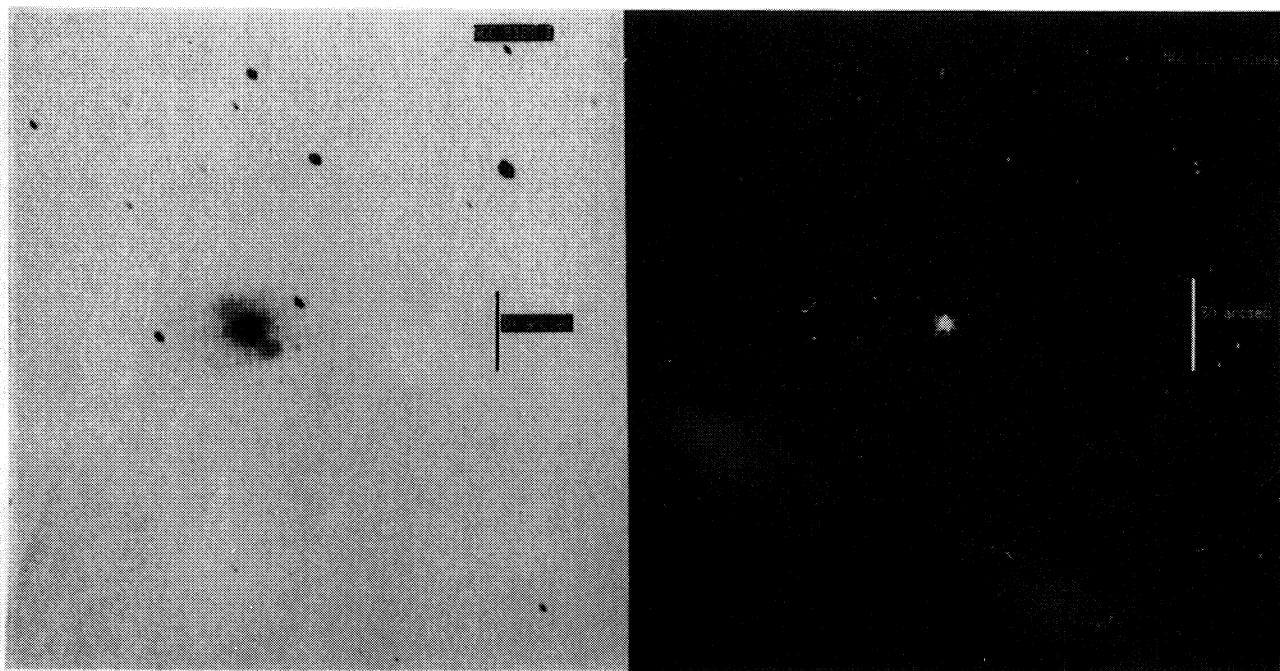Fig. 15. *I* and Hα images of NGC 2798. The vertical scale is 30″, north is up, east is left.
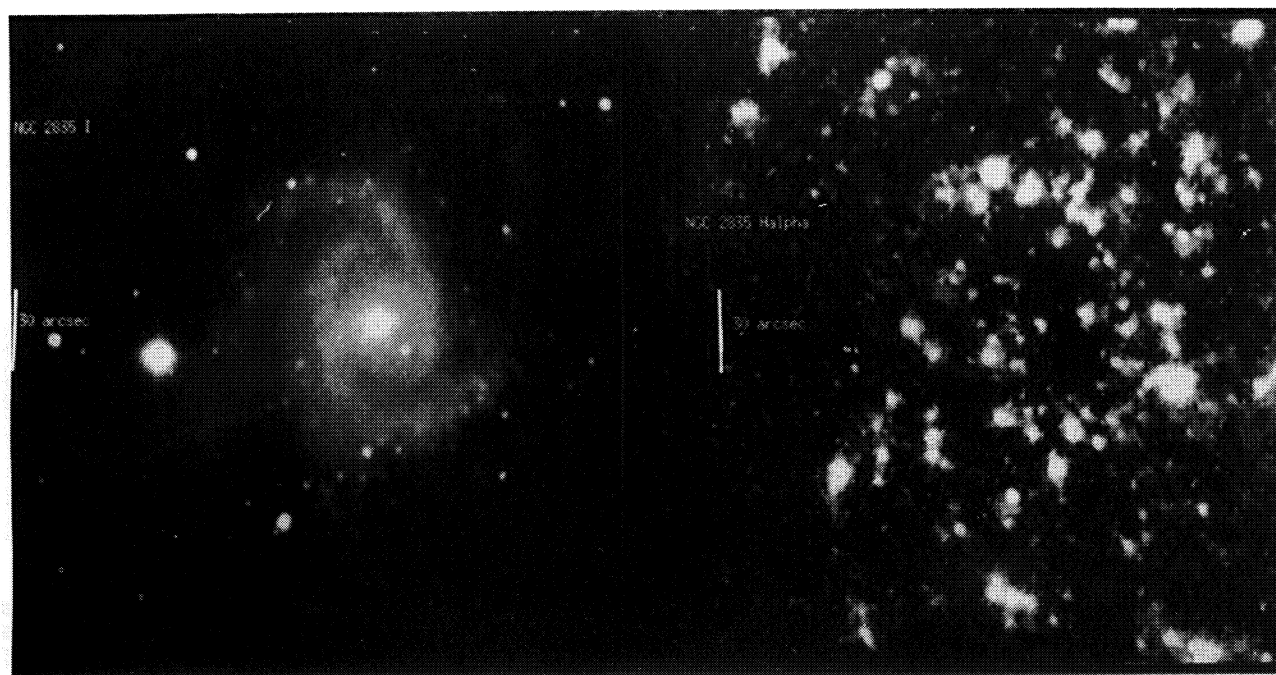
Fig. 16. *I* and Hα images of NGC 2835. The vertical scale is 30″, north is up, east is left.
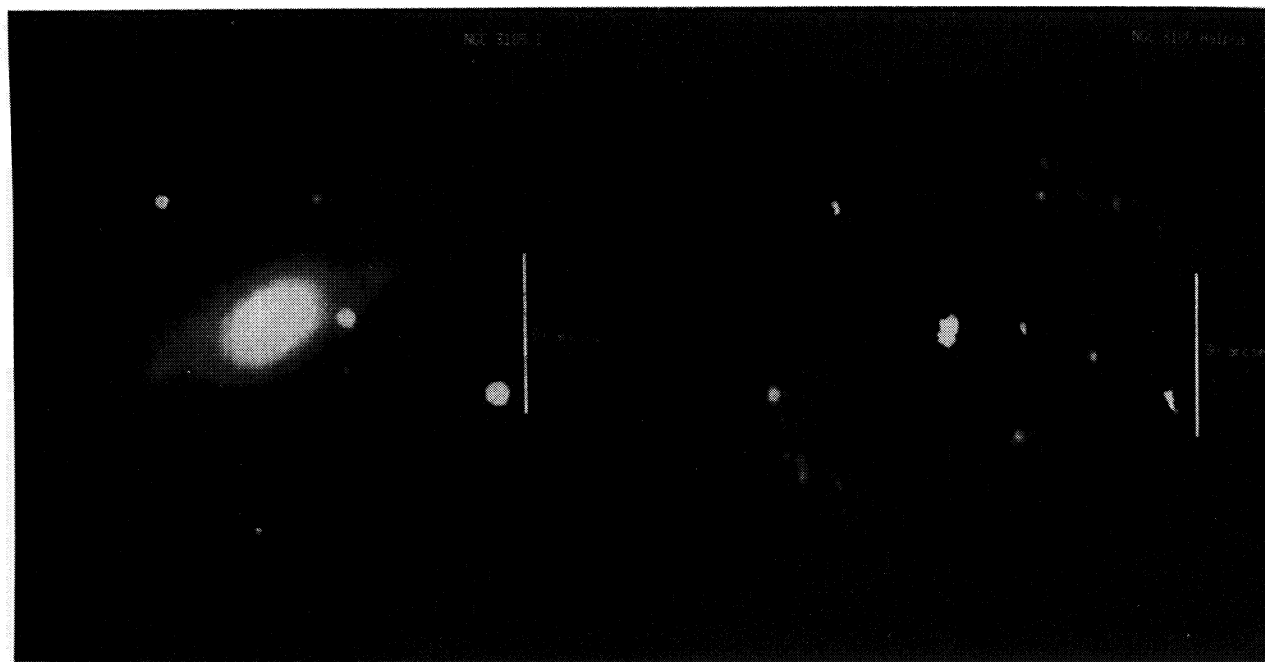
Fig. 17. *I* and Hα images of NGC 3185. The vertical scale is 30″, north is up, east is left.

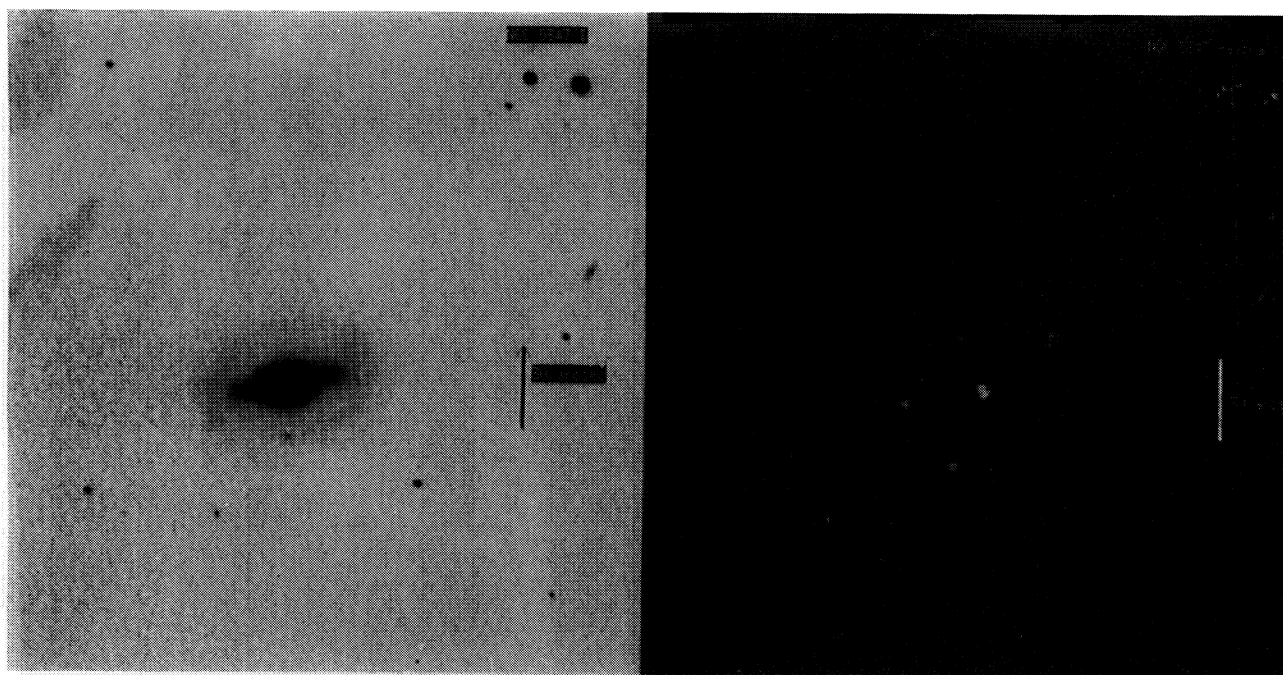Fig. 18. I and Hα images of NGC 3287. The vertical scale is 30″, north is up, east is left.

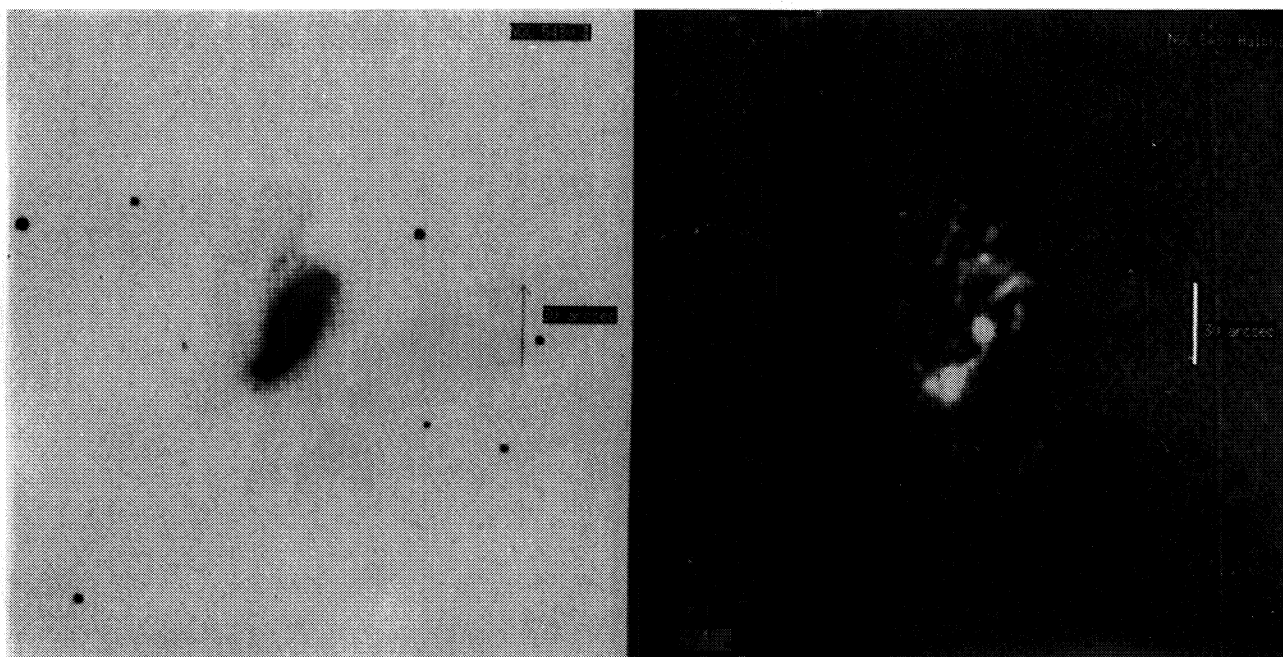Fig. 19. I and Hα images of NGC 3318. The vertical scale is 30″, north is up, east is left.

Fig. 20. *I* and Hα images of NGC 3319. The vertical scale is 30″, north is up, east is left.

Fig. 21. *I* and Hα images of NGC 3351. The vertical scale is 30″, north is up, east is left.

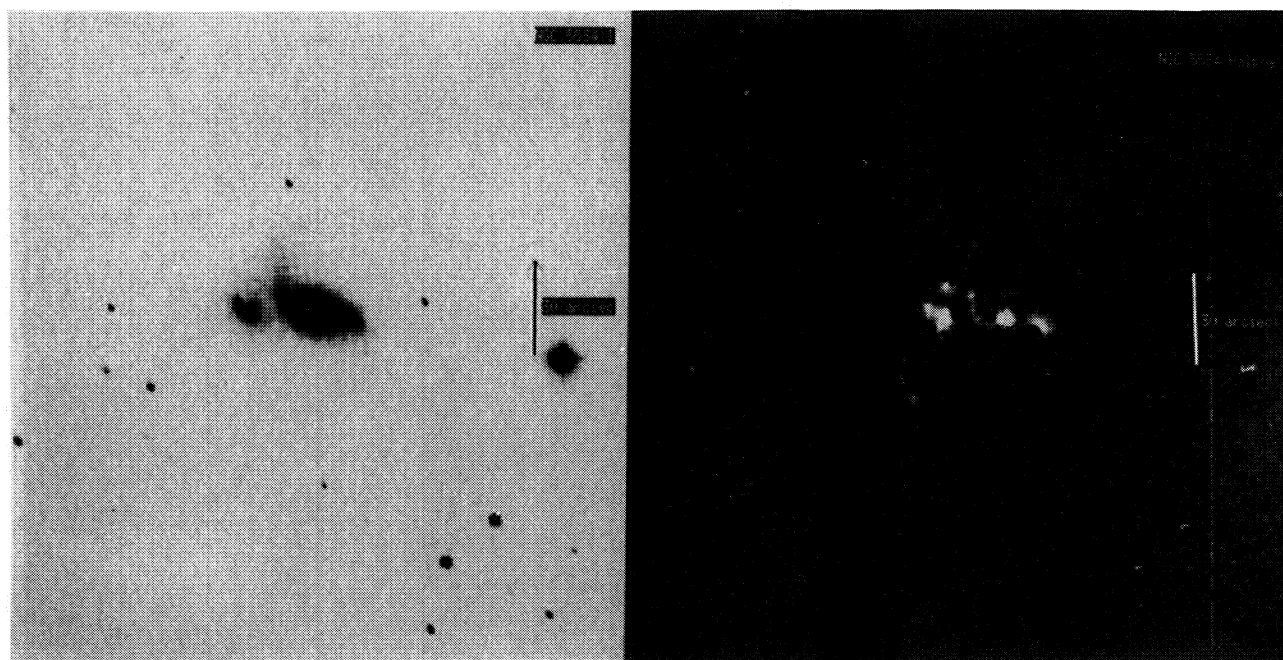Fig. 22. *I* and Hα images of NGC 3359. The vertical scale is 30″, north is up, east is left.

Fig. 23. *I* and Hα images of NGC 3367. The vertical scale is 30″, north is up, east is left.

Fig. 24. I and Hα images of NGC 3504. The vertical scale is 30$''$, north is up, east is left.

Fig. 25. I and Hα images of NGC 3513. The vertical scale is 30$''$, north is up, east is left.
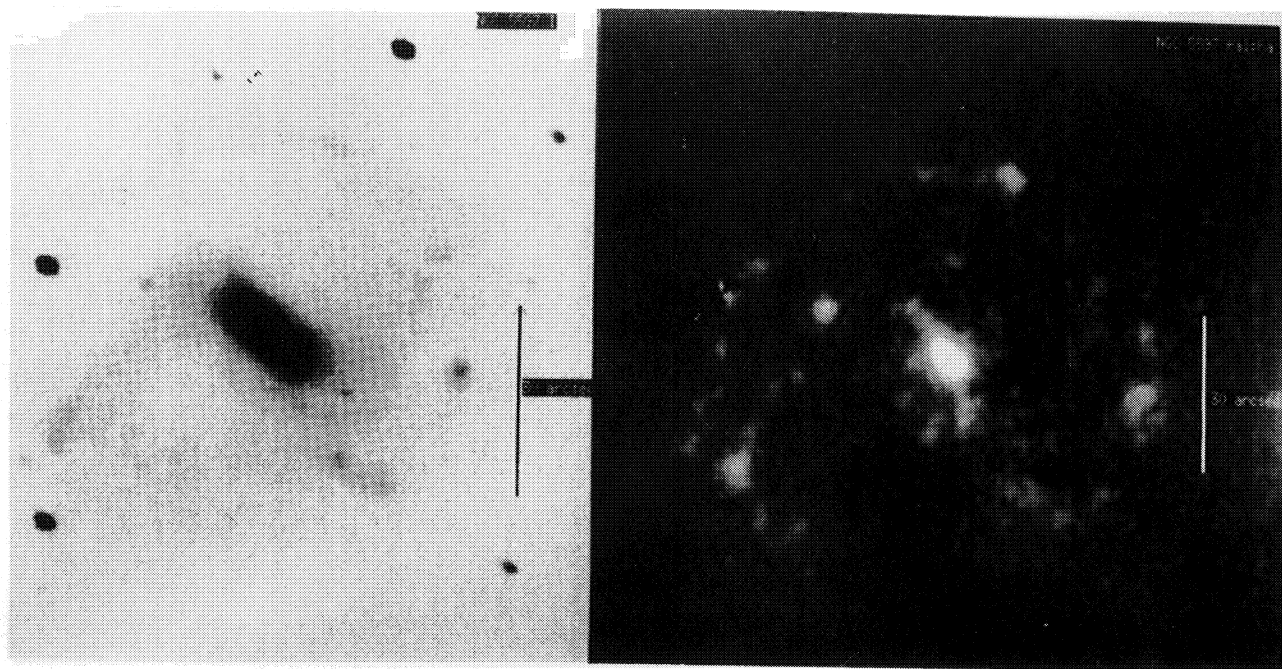
Fig. 26. *I* and Hα images of NGC 3783. The vertical scale is 30″, north is up, east is left.

Fig. 27. *I* and Hα images of NGC 3912. The vertical scale is 10″, north is up, east is left.

GARCÍA-BARRETO ET AL.

Fig. 28. *I* and Hα images of NGC 4123. The vertical scale is 30″, north is up, east is left.

Fig. 29. *I* and Hα images of NGC 4314. The vertical scale is 30″, north is up, east is left.

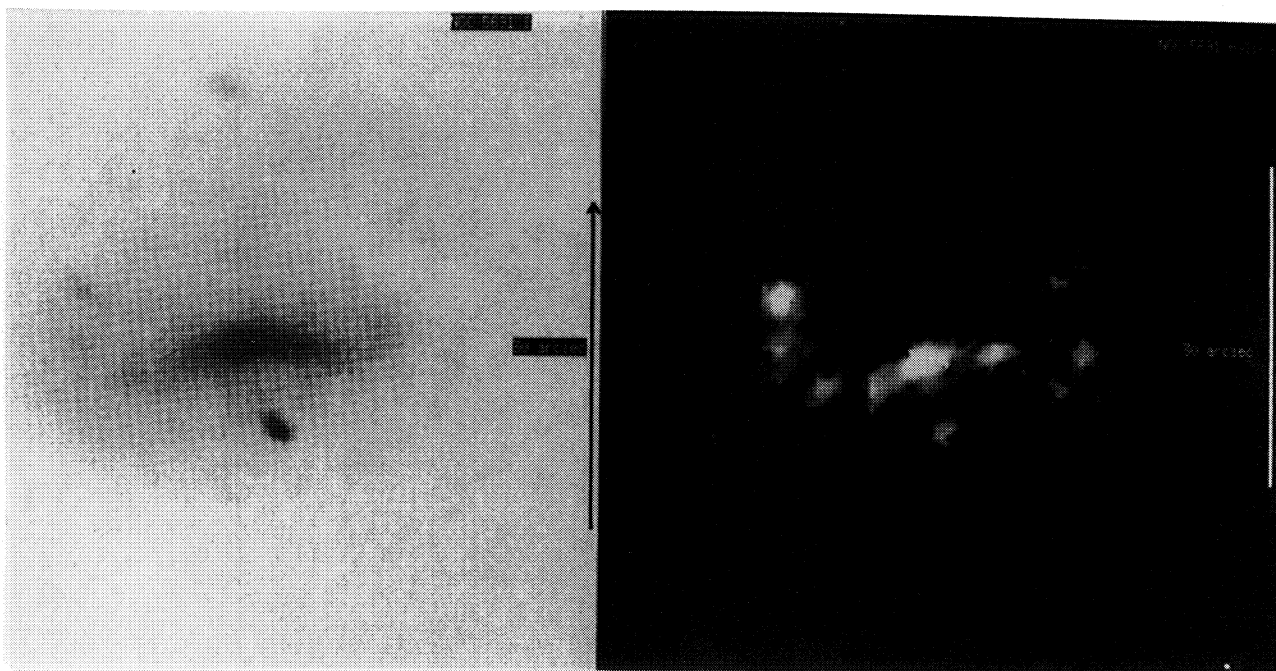Fig. 30. I and Hα images of NGC 4385. The vertical scale is 30″, north is up, east is left.

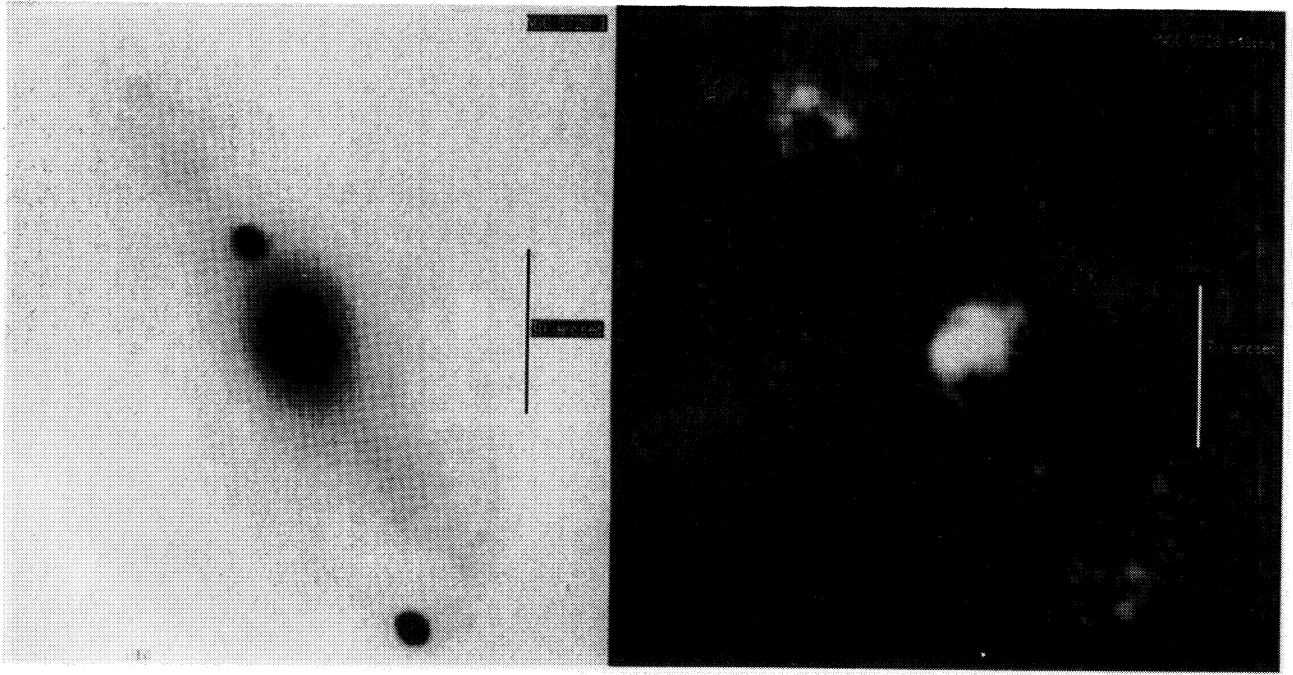Fig. 31 .I and Hα images of NGC 4507. The vertical scale is 10″, north is up, east is left.

Fig. 32. *I* and Hα images of NGC 4561. The vertical scale is 30″, north is up, east is left.

Fig. 33. *I* and Hα images of NGC 4688. The vertical scale is 30″, north is up, east is left.

Fig. 34. *I* and Hα images of NGC 4691. The vertical scale in the *I* image is 30″ while it is 10″ in the Hα image; north is up, east is left.

Fig. 35. *I* and Hα images of NGC 5135. The vertical scale is 30″, north is up, east is left.

Fig. 36. *I* and Hα images of NGC 5188. The vertical scale is 30″, north is up, east is left.

Fig. 37. *I* and Hα images of NGC 5347. The vertical scale is 30″, north is up, east is left.

Fig. 38. *I* and Hα images of NGC 5430. The vertical scale is 30″, north is up, east is left.

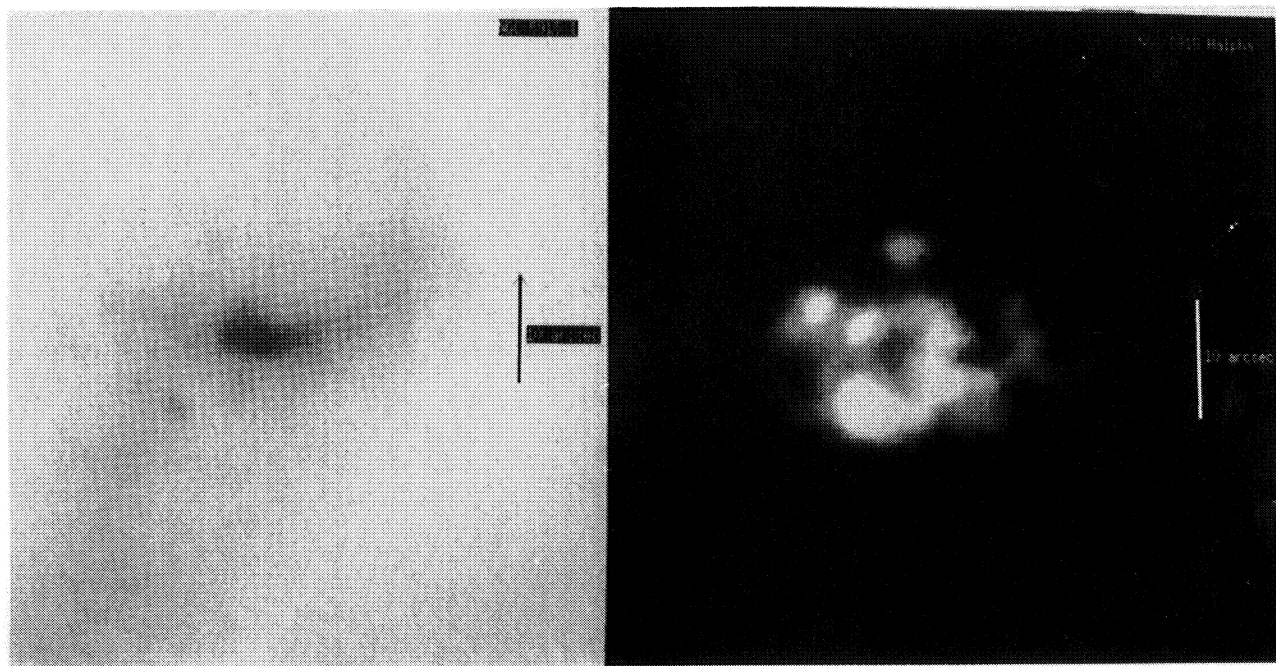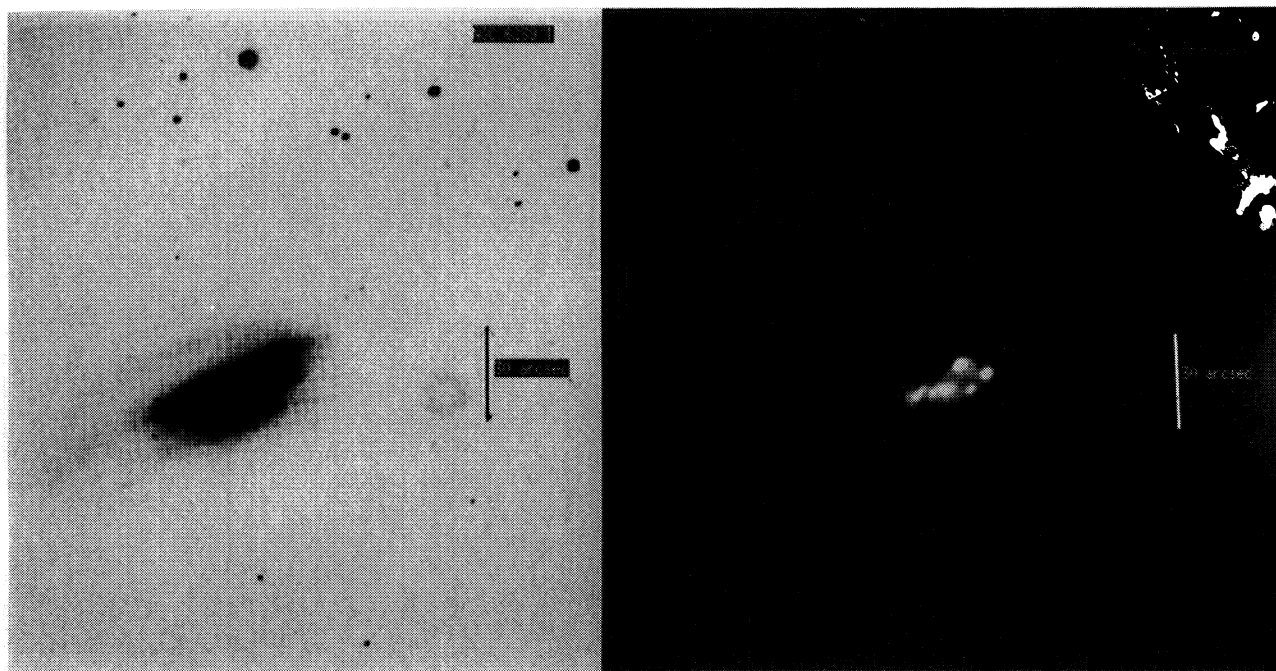Fig. 39. *I* and Hα images of NGC 5534. The vertical scale is 30″, north is up, east is left.

Fig. 40. *I* and Hα images of NGC 5597. The vertical scale is 30″, north is up, east is left.

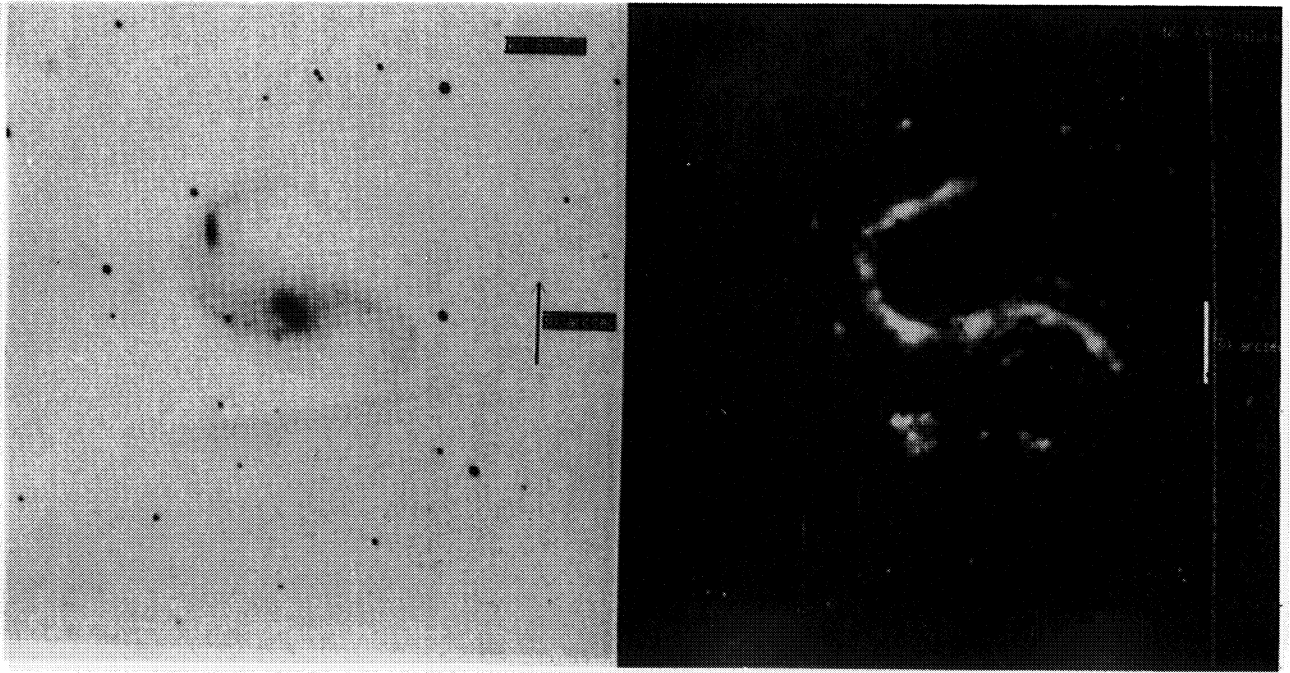Fig. 41. *I* and Hα images of NGC 5691. The vertical scale is 30″, north is up, east is left.

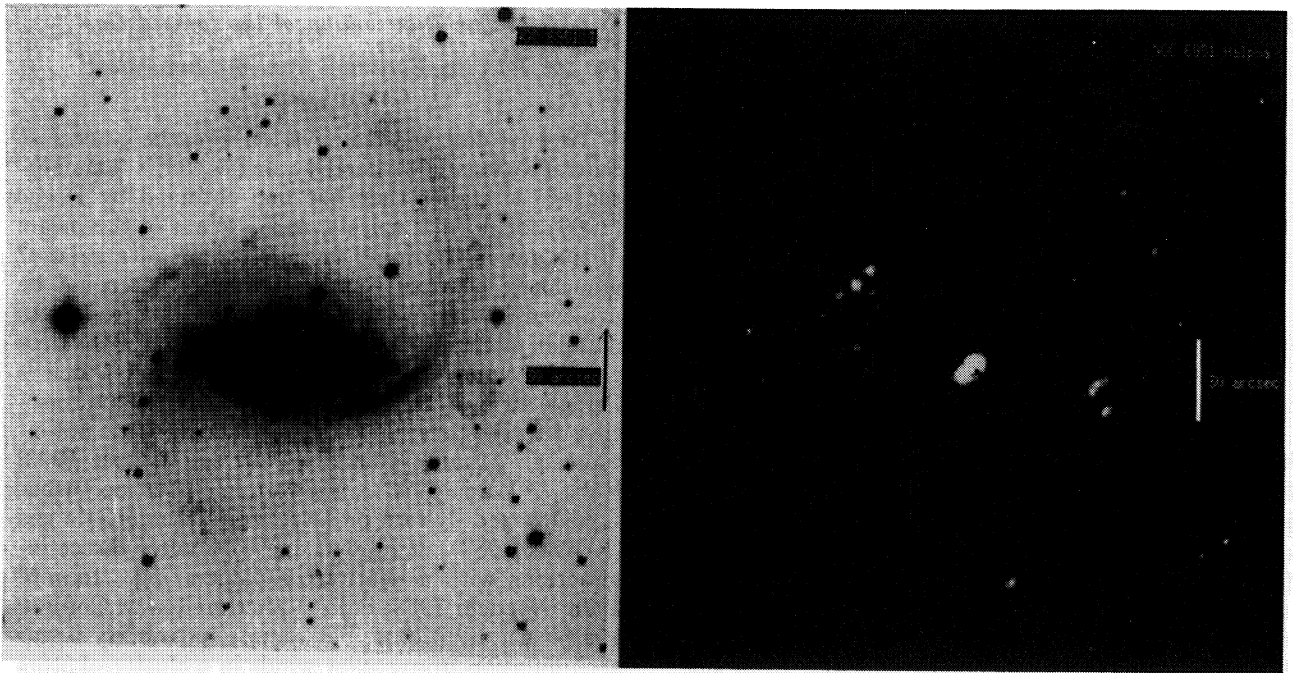Fig. 42. I and Hα images of NGC 5728. The vertical scale is 30″, north is up, east is left.
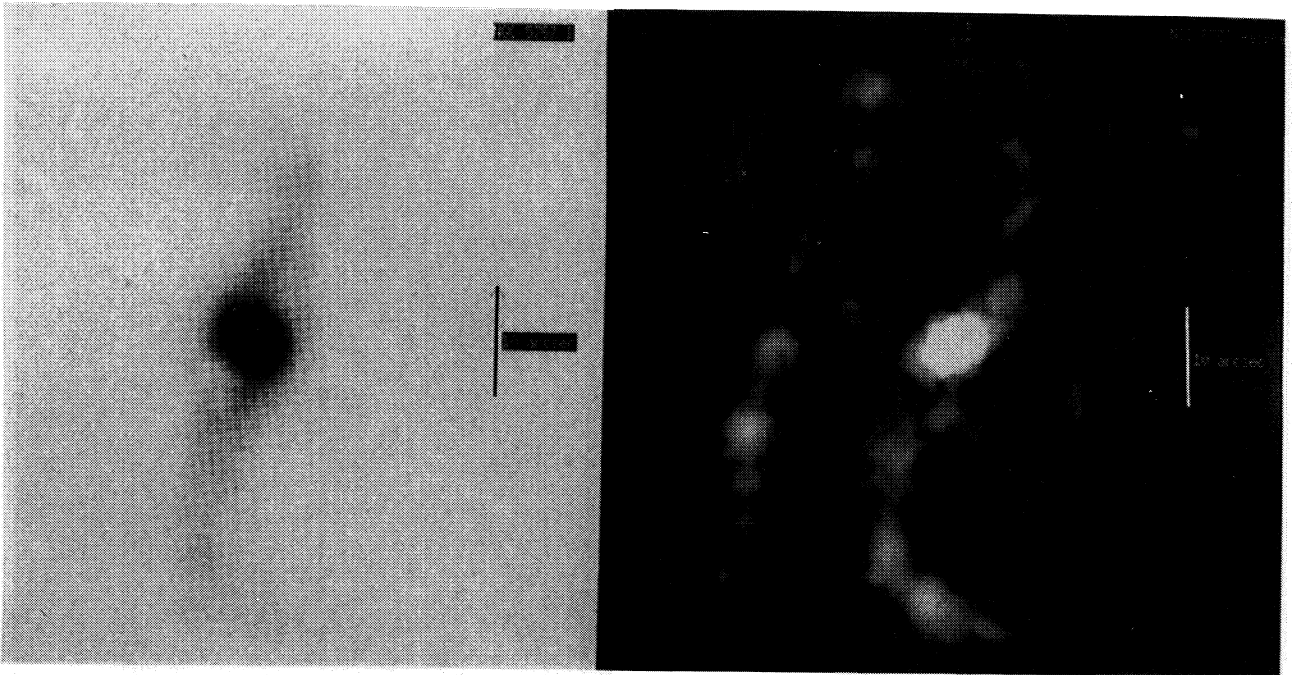
Fig. 43. I and Hα images of NGC 5757. The vertical scale is 10″, north is up, east is left.

Fig. 44. *I* and Hα images of NGC 5915. The vertical scale is 10″, north is up, east is left.

Fig. 45. *I* and Hα images of NGC 6239. The vertical scale is 30″, north is up, east is left.

Fig. 46. I and Hα images of NGC 6907. The vertical scale is 30″, north is up, east is left.

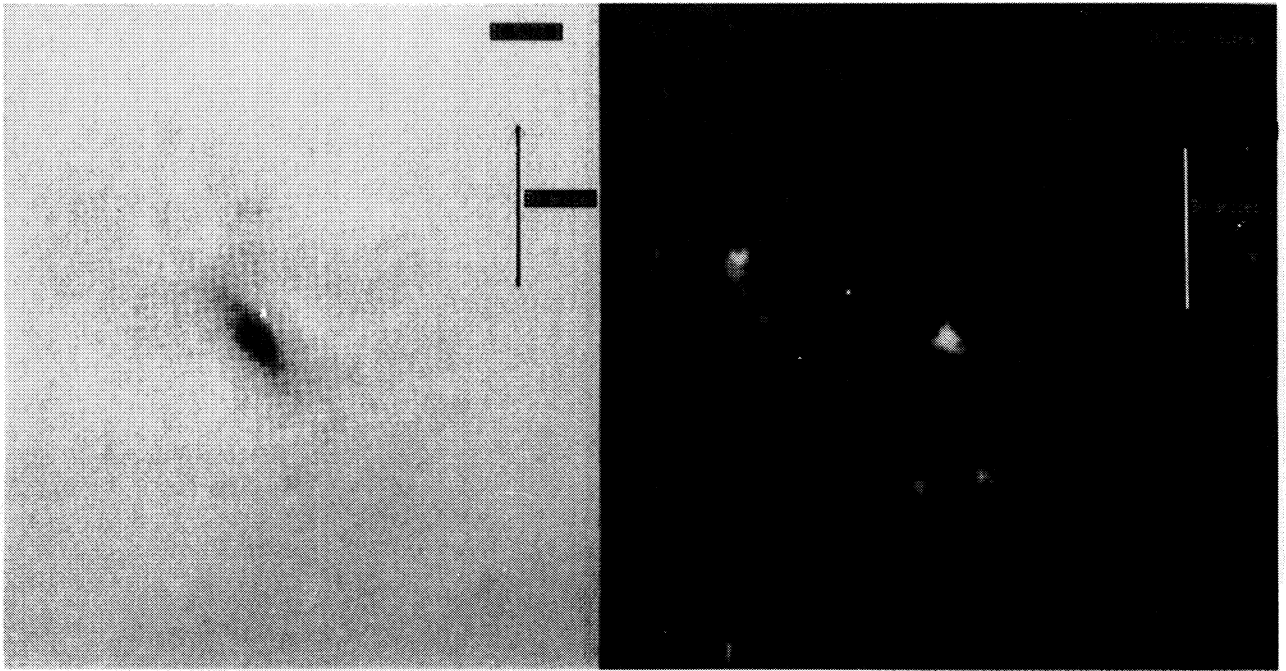Fig. 47. I and Hα images of NGC 6951. The vertical scale is 30″, north is up, east is left.

Fig. 48. *I* and Hα images of IC 5273. The vertical scale is 30″, north is up, east is left.

from giant H II regions at the disk, mainly in normal spiral arms. Three (6%) show Hα emission from the outer rings. Four (8%) present Hα emission from features in locations that are perpendicular to normal spiral arms, or to the bar. Finally, we did not detect any emission from 3 galaxies.

In one galaxy, NGC 3351, we detect emission from a series of different symmetric structures located at different radii. Also, NGC 4691 shows Hα emission from four bright knots in the central regions and a fast flow, possibly a result of compact SN embedded in dense environment (García-Barreto et al. 1995).

3. DISCUSSION

The Hα emission from giant H II regions is a good tracer of OB star formation. These regions also delineate the location of giant molecular clouds and, in our case, they show enhancements of the local gas density in resonance points, including the ends of the bars (e.g., Schwarz 1984; Combes & Gerin 1985; Binney & Tremaine 1987; Athanassoula 1992a,b). We concentrate in the distribution of ionized gas structures in barred galaxies, as the emission from the innermost central regions, rings (nuclear, inner and outer), the bar, and from locations perpendicular to the bar.

3.1. The Distribution of the Ionized Gas

3.1.1. Hα Emission from the Innermost Central Regions

We have detected Hα emission from the innermost central regions in 32 barred galaxies, 63%. This percentage is higher than the one obtained by Pogge (1989) for normal spirals, 41%. What is the origin of the gas in the inner few arcseconds of a galaxy? One likely possibility is gas inflow. This could be achieved by any combination of processes leading to angular momentum exchange in the disk of the host galaxy (Lynden-Bell & Kalnajs 1972; Lynden-Bell & Pringle 1974; Phinney 1994). There are inflows associated to the presence of a non-axisymmetric potential (e.g., Athanassoula 1992b; Friedli & Benz 1993; Habe & Wada 1993), inflows due to the perturbations exerted by ram pressure from intergalactic gas (Kritsuk 1983), or inflows due to tidal or direct interactions with a nearby companion (e.g., Toomre 1978; Noguchi 1988; Salo 1991; Horellou & Combes 1993). An additional, but remote, possibility is gas accumulation from stellar winds in a cluster of stars located near the nucleus. However, this case is very unlikely because, for typical mass loss rates from OB stars (i.e., $\sim 10^{-6}$ $M_\odot$ yr^{-1}) and a large number

of massive stars (i.e., $\sim 10^4$), one would need extremely long timescales to accumulate the amount of gas observed within the inner ~ 500 pc —i.e., between 10^8 to 10^9 $M_\odot$ in the cases of the Milky Way, NGC 1022, NGC 4314, and NGC 1530— (Bally et al. 1988; García-Barreto et al. 1991b,c; Downes et al. 1996). Thus, gas inflow due to angular momentum transfer seems to be the most important source of the interstellar components seen in the central regions of these barred galaxies.

We find as many *late* —1 SB(late)p, 9 SBc, 8 SBbc— as *early* —7 SBb, 1 SBab, 5 SBa— type barred spirals with ionized gas at their innermost central few arc-seconds. From our data we cannot differentiate if the emission comes from the compact nucleus or from a circumnuclear zone. Higher angular resolution observations reveal for example that the Hα emission in NGC 5728, an SBb galaxy of our sample, is weaker at the kinematical center than in nearby circumnuclear regions (Arribas & Mediavilla 1993). Driving gas from distances of several hundred parsecs to tens of parsecs from the compact nucleus requires additional mechanisms, and could be achieved by secondary bars (Phinney 1994; Ho 1994). In the case of the Milky Way, the gas observed in the central 7 pc from the center lies in a disk and is probably spiraling into the center (Ho 1994; Lacy 1994).

The existence of similar structures in other external galaxies will require *HST* observations to resolve them.

3.1.2. Hα Emission from Nuclear Rings

There are 10 galaxies with circumnuclear Hα emission, and most of them are earlier Hubble types; 3 are classified as SBa, 6 as SBb and 1 SBbc. Figures 49 to 59 show enlargements of the circumnuclear rings observed.

The dynamics under the influence of a non-axisymmetric potential results in density enhancements (for both gas and stars) at the resonant radii called Lindblad Resonances (Lindblad 1958; Binney & Tremaine 1987). In particular, for galaxies having relatively large mass concentrations in their central regions (i.e., with bulges) the inner Linblad resonance, ILR, can form structures near the compact nucleus. The observed relative distribution of circumnuclear rings among Hubble types, then, seems to be in agreement with these theoretical expectations because larger bulges are found in the earlier SBa and SBb types. This is reinforced by numerical simulations of galaxies with large bulge to disk mass ratios (i.e., early Hubble types) since they tend to form bars with large pattern speeds and a ring
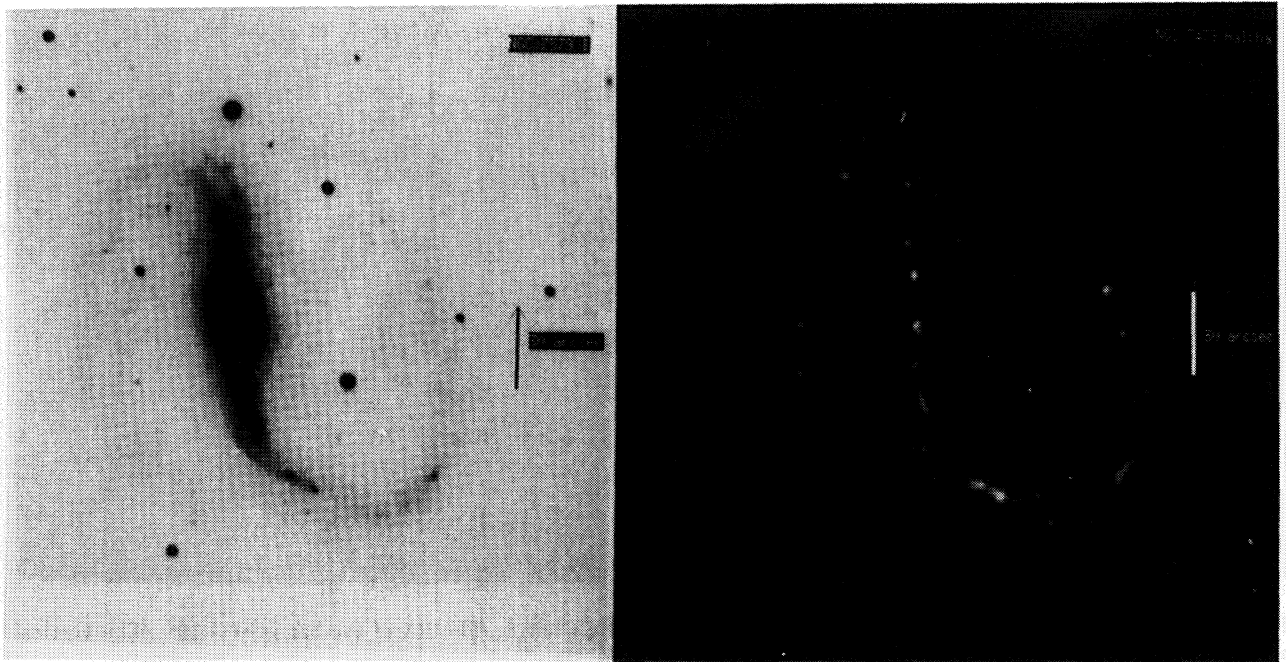

Fig. 49. *I* and Hα images of NGC 7479. The label in the *I* image indicates NGC 7579 but it is NGC 7479. The vertical scale is 30″, north is up, east is left.
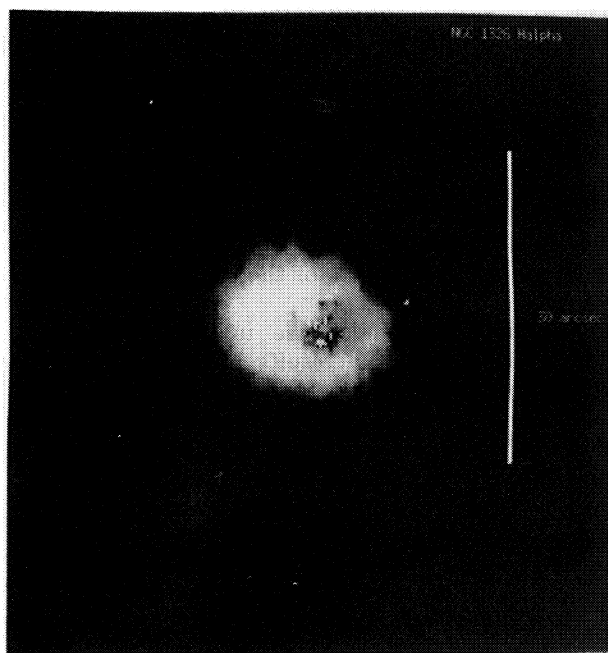
Fig. 50. Enlarged images of the Hα circumnuclear emission of NGC 1326. The PA of the bar is ∼20°. The vertical scale is 30″, north is up, east is left.

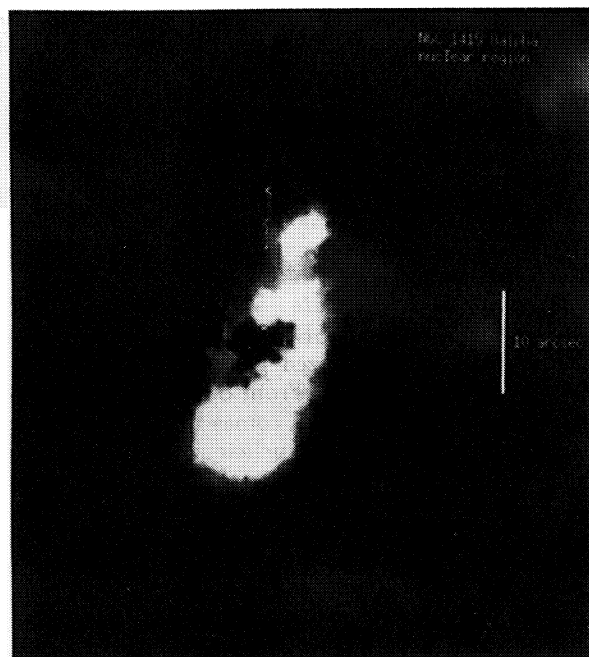Fig. 51. Enlarged images of the Hα circumnuclear emission of NGC 1415. The PA of the bar is ∼ − 50°. The vertical scale is 10″, north is up, east is left.
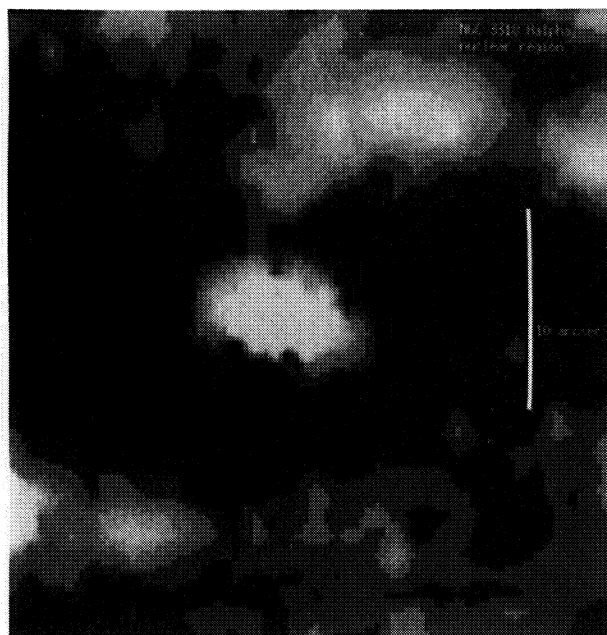

Fig. 52. Enlarged images of the Hα circumnuclear emission of NGC 3318. The PA of the bar is ∼ − 10°. The vertical scale is 10″, north is up, east is left.

Fig. 53. Enlarged images of the Hα circumnuclear emission of NGC 3351. The PA of the bar is ∼ − 70°. The vertical scale is 10″, north is up, east is left.

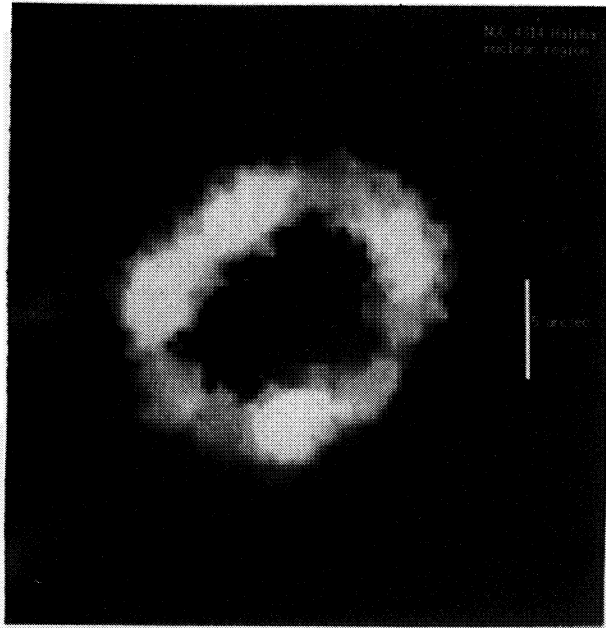Fig. 54. Enlarged images of the Hα circumnuclear emission of NGC 4314. The PA of the bar is ∼ − 35°. The vertical scale is 5″, north is up, east is left.

Fig. 55. Enlarged images of the Hα circumnuclear emission of NGC 5135. The PA of the bar is ∼ − 55°. The vertical scale is 5″, north is up, east is left.

Fig. 56. Enlarged images of the Hα circumnuclear emission of NGC 5347. The PA of the bar is ∼ − 80°. The vertical scale is 5″, north is up, east is left.

Fig. 57. Enlarged images of the Hα circumnuclear emission of NGC 5430. The PA of the bar is ∼ − 35°. The vertical scale is 5″, north is up, east is left.
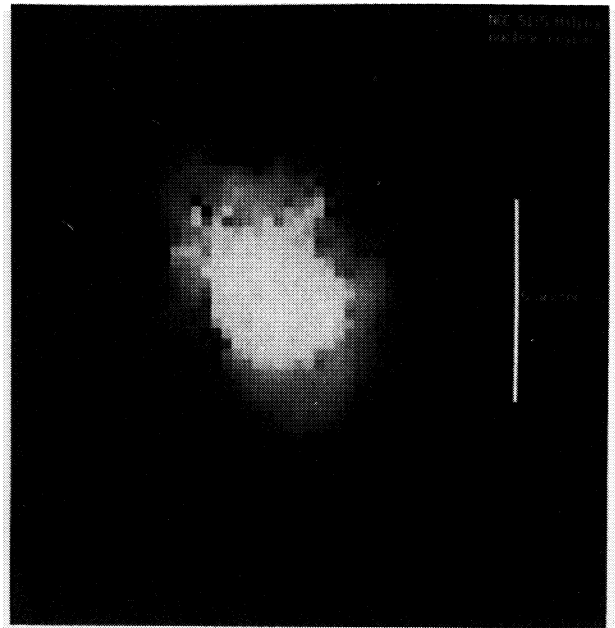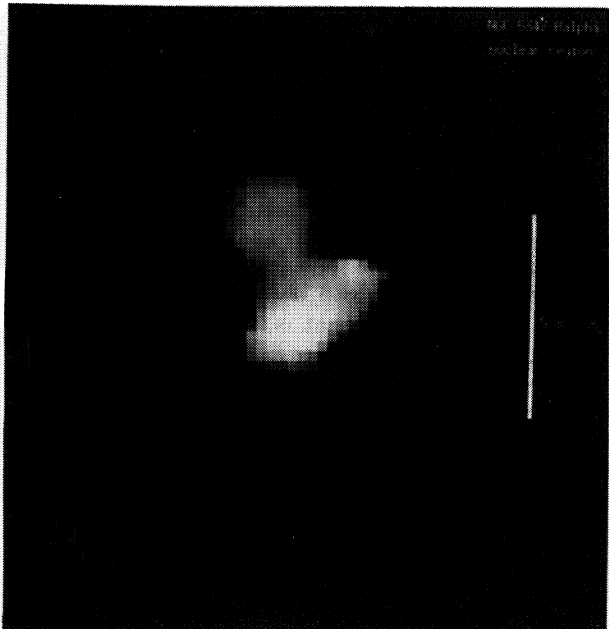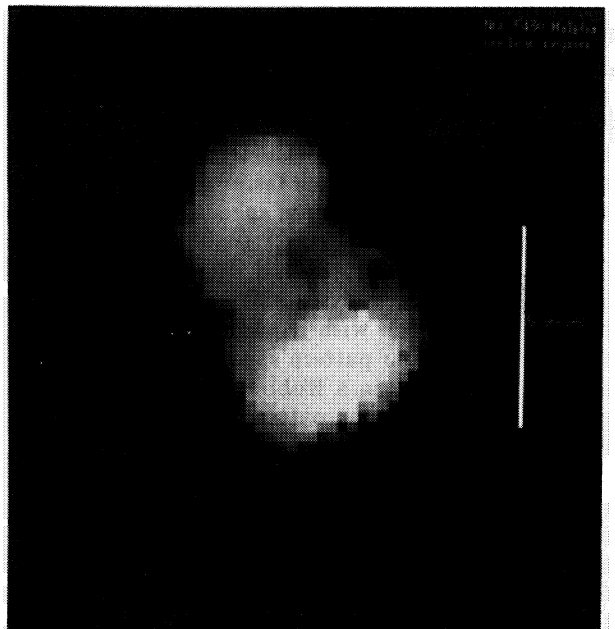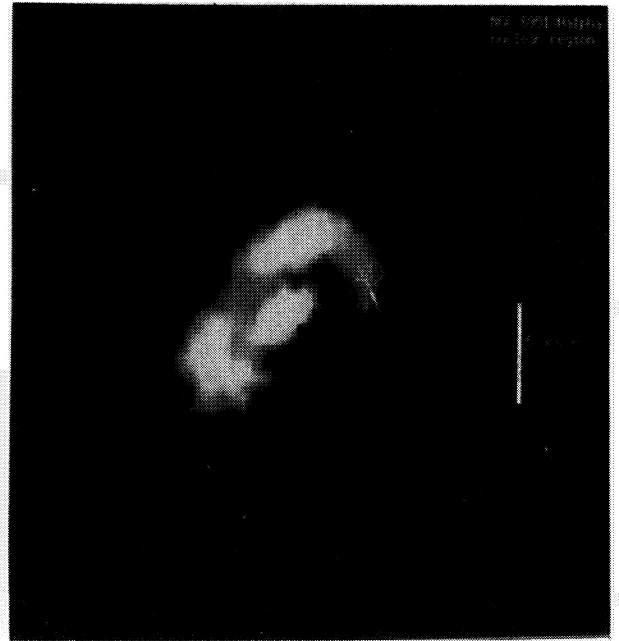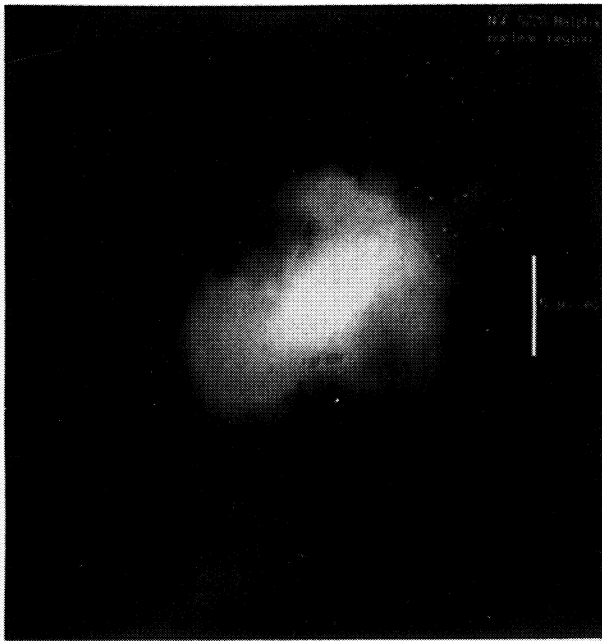
Fig. 58. Enlarged images of the Hα circumnuclear emission of NGC 5728. The PA of the bar is ~35°. The vertical scale is 5″, north is up, east is left.

Fig. 59. Enlarged images of the Hα circumnuclear emission of NGC 6951. The PA of the bar is ~85°. The vertical scale is 5″, north is up, east is left.

of both stars and gas is created at the ILR (e.g., Schwarz 1984; Combes & Gerin 1985; Contopoulos & Grösbol 1989; Athanassoula 1992b; Combes & Elmegreen 1993). The bar pattern speed, Ω_p, is related to the epicyclic frequency, κ, and angular velocity of the disk, Ω, such that $\Omega_p \lesssim \Omega - \kappa/2$. Thus, the bar cannot rotate much faster than the disk. Estimates of actual bar pattern speeds are in the range from $\Omega_p \simeq 19$ km s^{-1} kpc^{-1} to 90 km s^{-1} kpc^{-1} (García-Barreto et al. 1991a,b; Kenney et al. 1992; Telesco, Dressel & Wolstencroft 1993). In addition, N-body simulations with a pure stellar component suggest that the bar pattern speed can slow down by a factor of about 2 in a Hubble time but, when the gas is included, the bar pattern speed may increase with time (Athanassoula 1992b).

Unlike stars, gas clouds collide inelastically and then can drift into inner orbits. When the gas starts out in an x_1 orbit, it can interact with gas at the apocenter of an inscribed x_2 orbit and then settles down in the x_2 orbit (Binney et al. 1991). These interactions occur in the neighborhood of an ILR and may be the preferred locations for induced star formation (Kennicutt 1994). The observed orientations of the nuclear rings with respect to the orientation of the stellar bars are given in Table 5. On average, the relative angle difference is higher than 60°, and is in

agreement with the expected x_2 orbits, i.e., perpendicular to x_1 orbits, (Contopoulos & Grösbol 1989), indicating that the ILR was probably populated by the process described above (Athanassoula 1992a,b).

3.1.3. Hα Emission along Bars

We found 18 galaxies with Hα emission along the bar (i.e., with emission along the bar, but excluding the innermost central region). Four of them are classified as SBb and 1 as SB0/a, and 13 are classified as SBbc, SBc or SB late, that is, late type barred spirals. Only 3 of these galaxies have also nuclear rings. The observed emission in general consists of localized bright knots (e.g., NGC 4691, NGC 5915), with only a few cases with a smooth distribution (e.g., NGC 3504). The extent of a bar is determined by the disk length (Combes & Elmegreen 1993; Martin 1995), and a typical bar radius is of about 3 or 4 kpc. Thus, these knots (or the smooth emission) are spread over a wide range of galactocentric radii. The detection of ionized gas in the stellar bar region is certainly interesting, and is probably related with gas inflows.

There are two possible sources for the Hα emitting gas: photoionization or shock ionization. If star formation is taking place in the bar region, inflow ought

TABLE 5

RELATIVE ORIENTATION
AND SIZE OF NUCLEAR RINGS

Galaxy	Type	P.A. N.R.[a]	ΔPA^b	Size ($'' \times ''$)
NGC 1326	SBa	90°	70°	10×7.5
NGC 1415	SBa	170°	40°	8×8
NGC 3318	SBbc	80°	90°	7×2.5
NGC 3351	SBb	23°	93°	13×8
NGC 4314	SBa	140°	5°	13×10.7
NGC 5135	SBb	30°	85°	4.5×2.5
NGC 5347[c]	SBb	30°	110°	??×??
NGC 5430	SBb	25°	60°	5.2×2.3
NGC 5728	SBb	20°	15°	9×7[d]
NGC 6951	SBb	135°	50°	9×5

[a] Relative position angle of nuclear ring measured east of north. Estimated error is ± 5°.

[b] Position angle difference between the ring and the bar.

[c] There is Hα emission off nucleus to the NW and also to the NE. The position angle given here corresponds to the relative orientation of the NE extension off nucleus. The angular distance between nucleus and NE extension is about 2.5″.

[d] As reported by Wilson et al. 1993 with *HST* high resolution images since our resolution was not as good. Our Hα image show a more extended emission to the SE at PA $\simeq 120°$ coincident with the SE cone of high excitation gas observed by Schommer et al. 1988 and Wilson et al. 1993.

to be slow in order for clouds to coalesce, and ignite OB star formation (this occurs in time scales of a few times 10^7 yr; Casoli & Combes 1982; Franco 1993; Franco, Shore & Tenorio-Tagle 1994). If the gas is shock ionized, the shock velocities are expected to be in the range of 40 to 130 km s^{-1} (Shull & McKee 1979). In the presence of a bar, the gas cannot follow simple circular orbits and shocks occur. The simulations performed by Athanassuola (1992b) show regions along stellar bars with high mass densities corresponding to central shocks for late-type galaxies, and offset shocks on the leading edge for early-type galaxies. Our observations show bar emission mainly in late Hubble types, but cannot clarify if the gas is photo or shock ionized. This issue has to be addressed by additional observations in sulfur and nitrogen lines.

3.1.4. Hα Emission from Regions Perpendicular to the Bar

In NGC 1022 and NGC 3783, we have detected Hα emission from regions just outside the innermost central regions, but in directions perpendicular to

their stellar bars. For NGC 1022, the Hα feature extends to the north, whereas in NGC 3783 it extends to the east, to the west and probably to the SW of the galaxy.

In addition, there are a series of features in other galaxies (see figures): NGC 2139 shows Hα emission from the SE regions, suggesting a probable alignment with the center; NGC 2339 also shows emission from the SE regions, but now they are perpendicular to the spiral arms; NGC 2525 presents a double spiral arm in the south. NGC 3319 shows emission out of the bar, at the south east side; NGC 3513 similarly shows Hα straddling the bar, specially to the south. NGC 5728 presents extended Hα emission perpendicular to the bar, and its circumnuclear ring is aligned with the bar major axis (see also high resolution Hα emission images in Arribas & Mediavilla 1993 and Wilson et al. 1993). Finally, NGC 5915 seems to have a very weak emission from the innermost central region and shows bright Hα emission from the northern and southern adjacent regions.

Without any additional kinematic information, it is not clear whether the detected Hα emission from regions perpendicular to the bar corresponds to gas inflows or outflows. As stated before, inflows could be present in early type galaxies with x_2 orbits, which are located inside the central bulge and are aligned perpendicular to the bar (Athanassoula 1992a). This could be an explanation for the case of NGC 1022, but is unclear in the case of NGC 3783 since the emission extends all the way to the inner ring (and perhaps even beyond; see Figure 1b).

3.1.5. Hα Emission from Outer Rings

We have detected Hα emission from outer rings in only 3 galaxies. This result may be reflecting the well known fact that the star formation activity decreases with galactocentric radius. In addition, at large distances the environment could also play a role in determining a threshold for the formation of the ionizing OB stars. Also, possible absorption effects and our signal to noise ratio at these distances (i.e., low exposure times) might prevent us from detecting faint emission at the outer rings.

Dynamical models predict the location of the outer Lindblad Resonance, OLR, at a radius where $\Omega_p = \Omega + \kappa/2$, which is generally outside the radius of the stellar bar. An OLR could in principle exist for a given Ω_p and κ even if there is no ILR (Schwarz 1981; Combes & Gerin 1985; Contopoulos & Grösbol 1989).

3.2. Ionized Gas in Early-Type and Late-Type Galaxies

One clear, and probably important, result is that no Hα emission is detected from the bars of any galaxy classified as SBa. Eleven galaxies, out of a total of 52, are SBa. Six out of these 11 show emission

from their innermost central regions, 3 have nuclear rings, and 2 showed no Hα at all.

On the other hand, 28 out of the 52 galaxies, are classified as SBbc, SBc or SBlate. Eighteen out of these 28 (64%) show Hα emission from the innermost central regions. One galaxy, NGC 7479, shows emission along its bar in a straight and narrow region, but does not show any central emission. Thirteen out of the 28 (46%) have Hα from regions along their bars. In addition to our previous result, one can state that most of the galaxies with emission along the bar are classified as late-type.

Since later type galaxies have larger quantities of gas in their disks, these results may be simply associated to the fact that late type spirals have more gas available for inflows. If this is the case, it would be important to clarify two additional issues: a) one is the mass transfer rate in barred galaxies with different Hubble classification, and b) the time scale at which this transfer can occur. The simulations performed by Athanassuola (1992b) suggest a smaller mass inflow in late-type galaxies compared with early-type ones. This seems to be in contradiction with our results, unless the transfer timescales in early-type galaxies are very short. In addition, the viscosity and stability of a cloudy fluid are poorly known and can be strongly affected by the presence (and orientation) of a B-field (e.g., Franco, Santillán, & Martos 1995). The answer to these questions, then, require further observational and numerical studies.

3.3. Seyfert Galaxies

There are 8 Seyfert galaxies in our sample of barred spirals. Six are Sy 2, one is Sy 1, and one is classified as Sy-like. All of them show Hα emission from their inner few arc-seconds and, in addition, 5 of them are X-ray emitters. The galaxy with the strongest X ray emission, NGC 3783 (Sy 1), show Hα from regions perpendicular to its stellar bar (see Forte et al. 1987; Winge et al. 1992). NGC 5728 (Sy 2), also shows a complex Hα emission from circumnuclear regions, most likely including a southeast jet (Schommer et al. 1988, Wilson et al. 1993).

Earlier work by Simkin, Su, & Schwarz (1980) already indicated that the nuclear activity in Seyferts might be fed by gas from the disk, by inflows driven by a non-axisymmetric gravitational potential or by an external perturber. Presently, this view is supported by a large body of observational and theoretical results, and there is also ample evidence for induced star formation in the central regions of Seyferts (see recent review by Dultzin-Hacyan 1995). Obviously, the energy injected by young (or exploding) stars can generate vigorous outflows at the central regions (e.g., Heckman, Armus, & Miley 1987; Tomisaka 1994). Spectroscopic work done by Schommer et al. (1988) and Arribas & Mediavilla (1993)

suggest that in NGC 5728 both inflows and outflows from the nucleus can be occurring. As a comparison, another barred Sy 1.5 galaxy, NGC 1365, SBb(s), does have a circumnuclear radio continuum structure and probably an outflow jet (Sandqvist, Jörsäter, & Lindblad 1995) and it is an X ray emitter.

3.4. Spatial Distribution of Molecular Gas in Barred Galaxies

3.4.1. The Central Regions

For the molecular mass distribution, there are some apparent trends that are important to state here. In general, in luminous Sc galaxies the molecular gas is more abundant than the atomic component in the central regions, ≤ 1 kpc (Young & Scoville 1991). Given their modest angular resolution, however, the results from single dish studies cannot differentiate any of the possible existing components. Early single dish CO observations, with beam sizes above $12''$ in the CO(2−1) transition and above $20''$ in the CO(1−0) transition, give information about gas concentrations within kiloparsecs from the center, and high-resolution interferometric CO data are needed to unveil if the gas is concentrated or not at the compact nucleus.

For example, single dish observations with a resolution of $21''$ and $12''$ (García-Barreto et al. 1991b,a,c) indicated the presence of molecular gas in the inner regions of NGC 1022 (SBa pec), NGC 1326 (RSBa), and NGC 4314 (SBa), but high-resolution observations of NGC 4314 showed that the CO is circumnuclear without emission in the central $3''$ (Combes et al. 1992; Benedict, Smith, & Kenney 1996). Similarly, NGC 3351 SBb(r) and NGC 6951 SBbc(rs) have been observed with $2.4'' \times 2.3''$ and $2.3'' \times 2.1''$ CO beam sizes (Kenney et al. 1992), respectively, and do show a circumnuclear molecular gas structure but no emission at the compact nucleus. Another barred galaxy with similar properties (but is not in our sample) is NGC 1530 SBb(rs). It was observed with a $3.5'' \times 3.9''$ CO(1−0) beam size (Downes et al. 1996) and, again, does not show molecular emission at the nucleus but displays a circumnuclear structure probably coincident with an ILR.

There are some spiral galaxies with emission at the compact nucleus, but it is unclear how they relate with our sample. For instance, NGC 4321, a normal Sc observed with a $3.6'' \times 3.1''$ CO beam (Rand 1995), shows a central CO peak coincident with the optical compact nucleus in addition to a circumnuclear CO structure. NGC 1068, a Sb(rs), seems to have also molecular gas coincident with the compact nucleus (Planesas, Scoville, & Myers 1991; Kaneko et al. 1992). In the Sy 1 galaxy NGC 3227, the molecular gas concentration has two peaks straddling the optical Hα nucleus (Meixner et al. 1990),

while in the Sy 1 galaxy NGC 7469 there is definitely CO coincident within the $2''$ arc-sec resolution with the optical nucleus (defined by the peak in the red continuum). These two latter galaxies have close companions which could have most likely influenced the gas inflow all the way to the circumnuclear regions, and in NGC 7469 all the way to the compact nucleus. Detection of CO emission from the barred galaxy NGC 1365 (Sandqvist et al. 1995) indicates that gas is concentrated in the central region most probably originating from the circumnuclear radio continuum emission. Due to low angular resolution, nothing can be said on whether there is molecular gas from the compact nucleus. NGC 1365 is classified also as Sy 1.5 with a southeast jet (Sandqvist et al. 1995). CO has also been detected in the central regions (several hundred parsecs from the compact nucleus) of ultraluminous and distant galaxies (not necessarily barred), but their morphology suggests a merged phenomena (Scoville 1991; Downes, Solomon, & Radford 1993).

Single dish observations with a resolution of $55''$ indicate the presence of molecular gas in the inner regions of several galaxies of our sample; NGC 1022 (SBa), NGC 2339 (SBc), NGC 3359 (SBc), NGC 3504 (SBb), NGC 4385 (SBbc), NGC 4691 (SBa), and NGC 7479 (SBbc) (Young et al. 1995; Tinney et al. 1990).

3.4.2. Molecular Gas in the Nuclear Rings

Circumnuclear structures in CO have been detected with high angular resolution observations in several barred galaxies of our sample; NGC 3351 and NGC 6951 (Kenney et al. 1992), NGC 4314 (Combes et al. 1992; Benedict et al. 1996), and also in M101, NGC 1530 (Downes et al. 1996), NGC 1365 (Sandqvist et al. 1995) and NGC 2903 (Jackson et al. 1991).

It is important to note that the CO circumnuclear structure coincides well (within the errors) with the location of the Hα emission. This association suggest that the ionized gas traces well the star formation at or around the ILR.

3.4.3. Is There Molecular Gas along the Bars of Barred Galaxies?

In NGC 4691, the CO and Hα data in the bar region show strong peaks in the central regions, but the CO emission seems to straddle the inner Hα emission (Wiklind, Henkel, & Sage 1993; García-Barreto et al. 1995). Other barred galaxies also show CO along their bars; NGC 1097 (SBbc; Gerin et al. 1988), NGC 1530 (SBb; Downes et al. 1996), NGC 1365 (SBb; Sandqvist et al. 1995), NGC 2903 (SBab; Jackson et al. 1991), and M83 (SBc; Handa et al. 1990). Again, in NGC 2903 and M83, the Hα and CO structures are spatially correlated. The velocity deviations across the bar in M83 correspond to ~ 20

to 40 km s^{-1} in the plane of the galaxy, suggesting a flow towards the nucleus (Handa et al. 1990). In the bar of NGC 2903, the radio continuum at 21 cm, the CO, and the Hα emission are spatially associated. Outside the bar, the gas is predominantly atomic (Jackson et al. 1991). Further high-resolution studies will shed more light of the molecular gas distributions along stellar bars.

3.5. X Ray, Radio Continuum, and Dust Temperatures from Barred Galaxies

Is the Hα emission, specially from the innermost central regions, correlated with other global properties? From our observations, there is no apparent correlation between Hubble types and Hα emission from the central regions. If, as mentioned before, the disk gas is transported inwards from large radii, our observations indicate that the mechanism should be similar for all Hubble-types.

Is the environment important? Most of our galaxies with Hα emission from the central regions belong to clusters or groups (both compact and loose), but their images do not show clear signs of recent interactions (i.e., tidal tails or nearby optical companions, except for NGC 2798, NGC 3915, NGC 4435, and NGC 5597, that have companions at a distance of less than 5 galaxy diameters projected on the sky). There are also field galaxies (NGC 3367, NGC 4385, NGC 4561, NGC 5347, NGC 5534, NGC 5757, NGC 6239, and NGC 6951), that nevertheless have Hα at their centers. Thus, without quantitative measurements it is not clear to us how important is the surrounding medium compared to the intrinsic physical gravitational conditions of each galaxy. It would be useful to have more data about any surrounding gas, either hot (emitting in X rays) or cold (like H I clouds).

There is information in the far-infrared (from IRAS), radio continuum emission, and X rays (Fabbiano, Kim, & Trinchieri 1992) for some of the sample galaxies. Fifteen out of the 52 galaxies in our sample have reported X ray emission, and 10 out of these 15 show Hα from the central regions. In the case of NGC 3783, the peculiar Hα emission from the east and west sides of the nucleus has been reported by Forte et al. (1987) and Winge et al. (1992), and referred to it as the bridge emission. Spectroscopic studies show a broad Hα line, characteristic of a Seyfert galaxy, and a strong X ray emission (Evans 1988; Winge et al. 1992). Dust temperatures, assuming $S_\nu \simeq \lambda^{-1}$, is above 30 K in all galaxies with central Hα emission and X rays. We would like to call the attention of the reader on the observed characteristics of some galaxies: those that have a non-axysimmetric gravitational potential, have ionized gas at or around their compact nucleus, present nuclear activity as indicated by having broad Balmer lines and have X ray emission.

Low resolution radio continuum emission has been detected in ∼ 26 galaxies of our sample (Condon 1987; Condon et al. 1990; Condon & Broderick 1991). In some of them there are high resolution observations at two or three frequencies. For instance, in NGC 1022 the radio continuum emission comes from only two compact sources: one is associated with the innermost central region and the other one is at the north (García-Barreto et al. 1991c). Since the spectral index between 20 and 2 cm, computed with similar angular resolution at both wavelenghts, is flat, one can conclude that there is a recent burst of star formation as a result of a density enhancement (García-Barreto et al. 1991c). The radio continuum emission in NGC 1326, and NGC 4314 (García-Barreto et al. 1991a,b) comes from circumnuclear rings. In the case of NGC 1097 (not in our sample) there is radio continuum emission from a circumnuclear ring and also from an unresolved source with inverted spectral index at the nucleus (Hummel et al. 1987). Again, high resolution studies of the radio continuum emission from barred galaxies will be very useful in order to map its distribution, determine its spectral index with similar beams at different frequencies and to study any role of an existent magnetic field.

4. SUMMARY

We present the spatial distribution of the ionized gas, with CCD images in the narrowband filter Hα, for a sample of 52 bright barred spiral galaxies from the Shapley Ames Catalog. We also show images of the continuum emission in the broadband filter *I*. We detect Hα emission from several distinct regions: the innermost central regions, nuclear rings, inner rings, the bar, H II regions in the disk of galaxies, outer rings, and Hα features perpendicular to the bar or to normal spiral arms. An important result is that the galaxies with Hα emission along the bars are classified as late-type, and no galaxy classified as SBa showed this emission.

We believe that our set of images are a good source of information of the spatial distribution of ionized gas in barred galaxies. Our observations were not calibrated in flux nor in magnitude and, although the seeing conditions were good (1″ to 1.3″) during each night of observation, we are aware that absorption effects and the modest signal to noise ratio in some cases could affect the final images and some details of our analysis of the ionized gas spatial distribution. With this in mind, for our sample of 52 galaxies, the summary of observations indicates the following distributions: a) 32 galaxies show Hα emission from the innermost central regions, i.e., from the inner 5″, b) 10 have nuclear rings, c) 18 show emission along the bar, d) 18 show emission from the end of the bar, e) 26 have emission from H II regions in the disk

—normal spiral arms—, f) 9 have inner rings, g) 3 have outer rings, h) 4 have emission from locations perpendicular either to normal spiral arms and/or to the bar, i) 3 galaxies do not have detectable Hα emission. In only one galaxy, NGC 3351 SBb, there is emission at all rings, (nuclear, inner, and outer), but shows no Hα emission from the innermost central region. We found no correlation between Hα from the innermost central region and Hubble type. Out of the 32 galaxies with Hα emission from the innermost central region, 4 have also emission from circumnuclear rings, and 12 from regions along the bar. No emission was detected from the bars of any galaxy classified as SBa. Instead, most of the galaxies with Hα emission along their bars are classified as late type.

More high-resolution observations are needed in order to map the molecular gas and search for correlations between Hα and molecular emissions. We encourage further observational and numerical studies of the dynamics of barred galaxies with different Hubble types. In particular, additional models including both stars *and gas* in the presence of a companion, or a perturber, will shed more light on the response of bars to strong interactions (e.g., Salo, García-Barreto & Franco 1996).

REFERENCES

Arribas, S., & Mediavilla, E. 1993, ApJ, 410, 552
Arsenault, R., Boulesteix, J., Georgelin, Y., & Roy, J.-R. 1988, A&A, 200, 29
Athanassoula, E. 1984, Phys. Rep., 114, 319
_____. 1992a, MNRAS, 259, 328
_____. 1992b, MNRAS, 259, 345
Bally, J., Stark, A.A., Wilson, R.W., & Henkel, C. 1988, ApJ, 324, 223
Benedict, G.F., Smith, B.J., & Kenney, J.D.P. 1996, in IAU Colloq. 157, Barred Galaxies, ed. R. Buta, D.A. Crocker, & B.G. Elmegreen, Astron. Soc. Pac. Conf. Series, 227
Binney, J. & Tremaine, S. 1987, Galactic Dynamics (New Jersey: Princeton Univ. Press)

Binney, J., Gerhard, O.E., Stark, A.A., Bally, J., & Uchida, K.I. 1991, MNRAS, 252, 210

Buta, R. 1986, ApJS, 61, 639

_____. 1995, ApJS, 96, 39

Buta, R., & Crocker, D.D. 1991, AJ, 102, 1715

Casoli, F., & Combes, F. 1982, A&A, 110, 287

Combes, F., & Elmegreen, B. 1993, A&A, 271, 391

Combes, F., & Gerin, M. 1985, A&A, 150, 327

Combes, F., Gerin, M., Nakai, N., Kawabe, R., & Shaw, M. A. 1992, A&A, 259, L27

Condon, J.J. 1987, ApJS, 65, 485

Condon, J.J., & Broderick, J.J., 1991, AJ, 102, 1663

Condon, J.J., Helou, G., Sanders, D.B., & Soifer, B.T. 1990, ApJS, 73, 359

Contopoulos, G. 1980, A&A, 81, 198

Contopoulos, G., & Grösbol, P. 1989, A&AR, 1, 261

Downes, D., Solomon, P.M., & Radford, S.J.E. 1993, ApJ, 414, L13

Downes, D., Reynaud, D., Solomon, P.M., & Radford, S.J.E. 1996, ApJ, in press

Dultzin-Hacyan, D. 1995, in The Fifth Mexico-Texas Conference on Astrophysics: Gaseous Nebulae and Star Formation, ed. M. Peña & S. Kurtz, RevMex-AASC, 3, 31

Escalante-Ramíirez, B., & Martens, J.-B. 1992, J. Visual Comm. & Imag. Represent., 3, 272

Evans, I.N. 1988 ApJS, 67, 373

Fabbiano, G., Kim, D.-W., & Trinchieri, G. 1992, ApJS, 80, 531

Forte, J., Vega, E.I., Calderon, J.H., & Feinstein, F. 1987, AJ, 92, 301

Franco, J. 1993, RevMexAA, 26, 13

Franco, J., Shore, S.N., & Tenorio-Tagle, G. 1994, ApJ, 436, 795

Franco, J., Santillán, A., & Martos, M. 1995, in Formation of the Milky Way, ed. E. Alfaro & A. Delgado, (Cambridge: Cambridge Univ. Press), 97

Friedli, D., & Benz, W. 1993, A&A, 268, 65

García-Barreto, J.A., Franco, J., & Carrillo, R. 1996, ApJ, 469, in press

García-Barreto, J.A., Carrillo, R., Klein, U., & Dahlem, M. 1993, RevMexAA, 25, 31

García-Barreto, J.A., Franco, J., Guichard, J., & Carrillo, R. 1995, ApJ, 451, 156

García-Barreto, J. A., Dettmar, R.-J., Combes, F., Gerin, M., & Koribalski, B. 1991a, RevMexAA, 22, 197

García-Barreto, J.A., Downes, D., Combes, F., Carrasco, L., Gerin, M., & Cruz-González, I. 1991c, A&A, 252, 19

García-Barreto, J.A., Downes, D., Combes, F., Gerin, M., Magri, C., Carrasco, L., & Cruz-González, I. 1991b, A&A, 244, 257

Gerin, M., Nakai, N., & Combes, F. 1988, A&A, 203, 44

Habe, A., & Wada, K. 1993, in Star Formation, Galaxies and the Interstellar Medium, ed. J. Franco, F. Ferrini, & G. Tenorio-Tagle (Cambridge: Cambridge Univ. Press), 134

Handa, T., Nakai, N,, Sofue, Y., Hayashi, M., & Fujimoto, M. 1990, PASJ, 42, 1

Hawarden, T.G., Mountain, C.M., Leggett, S.K., & Puxley, P.J., 1986, MNRAS, 221, 41

Heckman, T.M., Armus, L., & Miley, G.K. 1987, AJ, 93, 276

Helou, G. 1986, ApJ, 311, L33

Ho, P.T.P. 1994, in The Nuclei of Normal Galaxies: Lessons from the Galactic Center, ed. R.Genzel & A.I. Harris, (Dordrecht: Kluwer), p. 149

Hodge, P.W., & Kennicutt, R.C. 1983, AJ, 88, 296

Horellou, C., & Combes, F. 1993, in N body Problems and Gravitational Dynamics, ed. F. Combes & E. Athanassoula, (Aussois, Haute Maurienne, France), 168

Hummel, E., van der Hulst, J.M., & Keel, W.C. 1987, A&A, 172, 32

Jackson, J.M., Eckart, A., Cameron, M., Wild, W., Ho, P.T.P., Pogge, R.W., & Harris, A.I. 1991, ApJ, 375, 105

Kaneko, N., Morita, K., Fukui, Y., Takahashi, N., Sugitani, K., Nakai, N., & Morita, K.-I. 1992, PASJ, 44, 341

Keel, W.C. 1983, ApJ, 268, 632

Keel, W.C., Kennicutt, R.C., Hummel, E., & van der Hulst, J.M. 1985, AJ, 90, 708

Kennicutt, R.C. 1994, in Mass Transfer Induced Activity in Galaxies, ed. I. Shlosman (Cambridge: Cambridge Univ. Press), 131

Kennicutt, R.C., & Kent, S.M. 1983, AJ, 88, 1094

Kenney, J.D.P., Wilson, C.D., Scoville, N.Z., Deveroux, N., & Young, J.S. 1992, ApJ, 395, L79

Kritsuk, A.G. 1983, Afz., 19, 263

Lacy, J.H. 1994, in The Nuclei of Normal Galaxies: Lessons from the Galactic Center, ed. R. Genzel & A.I. Harris (Dordrecht: Kluwer), 165

Lindblad, B. 1958, Stockholm Annaler, 20, 6

Lynden-Bell, D., & Kalnajs, A.J. 1972, MNRAS, 157, 1

Lynden-Bell, D., & Pringle, J.E. 1974, MNRAS, 168, 603

Martin, P. 1995, AJ, 109, 2428

Meixner, M., Puchalsky, R., Blitz, L., Wright, M., & Heckman, T. 1990, ApJ, 354, 158

Noguchi, M. 1988, A&A, 203, 259

Nordgren, T.E., Helou, G., Chengalur, J.N., Terzian, Y., & Khachikian, E. 1995, ApJS, 99, 461

Phinney, E.S. 1994, in Mass Transfer Induced Activity in Galaxies, ed. I. Shlosman (Cambridge: Cambridge Univ. Press), 1

Planesas, P., Scoville, N.Z., & Myers, S.T. 1991, ApJ, 369, 364

Pogge, R.W. 1989, ApJS, 71, 433

Rand, R.J. 1995, AJ, 109, 2444

Ryder, S.D., & Dopita, M.A. 1993, ApJS, 88, 415

Salo, H. 1991, A&A, 243, 118

Salo, H., García-Barreto, J.A. & Franco, J. 1996, in preparation

Sandage, A., & Tammann, G.A. 1981, A Revised Shapley-Ames Catalog of Bright Galaxies (Washington, D.C.: Carnegie Inst. of Washington)

Sandqvist, A., Jörsäter, S., & Lindblad, P.O. 1995, A&A, 295, 589

Schwarz, M.P. 1981, ApJ, 247, 77

_____. 1984, MNRAS, 209, 93

Schommer, R.A., Caldwell, N., Wilson, A.S., & Baldwin, J.A., 1988, ApJ, 324, 154

Scoville, N.Z. 1991 in IAU Symp. 146, Dynamics of Galaxies and their Molecular Cloud Distributions, ed. F. Combes & F. Casoli (Dordrecht: Reidel), 315

Shull, J.M., & Mckee, C.F. 1979, ApJ, 227, 131

Simkin, S.M., Su, H.J., & Schwarz, M.P. 1980, ApJ, 237, 404

Telesco, C.M., Dressel, L.L., & Wolstencroft, R.D. 1993, ApJ, 414, 120

Tinney, C.G., Scoville, N.Z., Sanders, D.B., Soifer, B.T. ˙1990, ApJ, 362, 473

Tomisaka, K. 1994, in Numerical Simulations in Astrophysics, ed. J. Franco, S. Lizano, L. Aguilar, & E. Daltabuit (Cambridge: Cambridge Univ. Press), 184

Toomre, A. 1978, in IAU Symp. 79, The Large Scale Structure of the Universe, ed. M.S. Longair & J. Einasto (Dordrecht: Reidel), 109

Wiklind, T., Henkel, C., & Sage, L.J. 1993, A&A, 271, 71

Wilson, A.S., Braatz, J.A., Heckman, T.M., Krolik, J.H., & Miley, G.K. 1993, ApJ, 419, L61

Winge, C., Pastoriza, M.G., Storchi-Bergmann, T., & Lipari, S. 1992, ApJ, 393, 98

Young, J.S., & Scoville, N.Z. 1991, ARA&A, 29, 581

Young, J.S. et al. 1995, ApJS, 98, 219

José Franco, José A. García-Barreto, and René Carrillo: Instituto de Astronomía, UNAM, Apartado Postal 70-264, 04510 México, D.F., México. (tony@astroscu.unam.mx).

B. Escalante-Ramírez and S. Venegas: División de Estudios de Posgrado, Facultad de Ingeniería, UNAM, Apartado Postal 70-256, México, D.F., México.